Onorati M, Li Z, Liu FC, Sousa AMM, Nakagawa N, Li MF, Dell'Anno MT, Gulden FO, Pochareddy S, Tebbenkamp ATN, Han WQ, Pletikos M, Gao TLY, Zhu Y, Bichsel C, Varela L, Szigeti-Buck K, Lisgo S, Zhang YL, Testen A, Gao XB, Mlakar J, Popovic M, Flamand M, Strittmatter SM, Kaczmarek LK, Anton ES, Horvath TL, Lindenbach BD, Sestan N. Zika Virus Disrupts Phospho-TBK1 Localization and Mitosis in Human Neuroepithelial Stem Cells and Radial Glia. *Cell Reports* 2016, 16(10), 2576-2592.

Article

Cell Reports

Zika Virus Disrupts Phospho-TBK1 Localization and Mitosis in Human Neuroepithelial Stem Cells and Radial Glia

Graphical Abstract

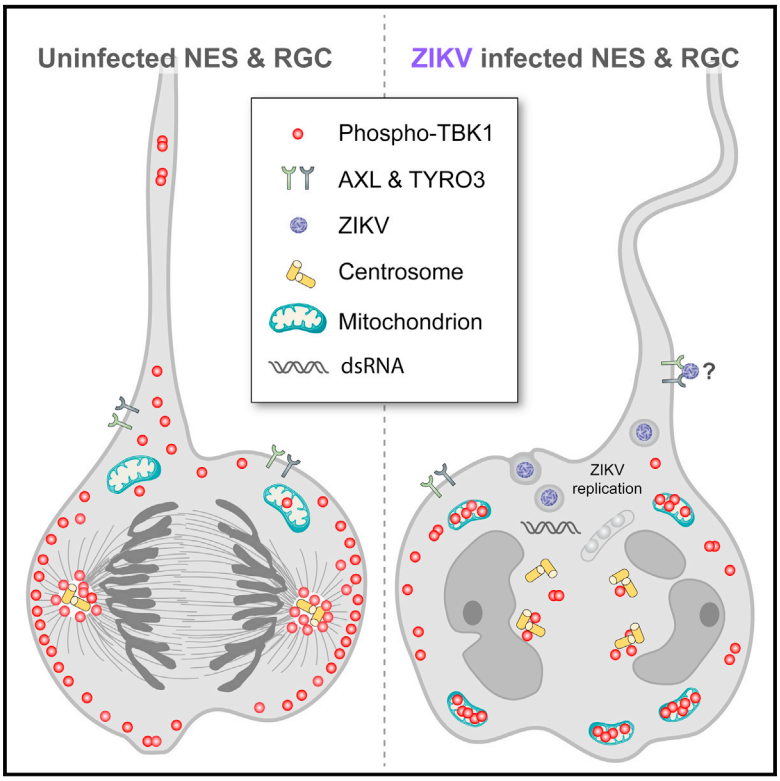

Highlights

- Derivation of human neocortical and spinal cord neuroepithelial stem (NES) cells
- Zika virus (ZIKV) infects NES cells and radial glia, impairing mitosis and survival
- ZIKV induces mitochondrial sequestration of centrosomal phospho-TBK1
- Nucleoside analogs inhibit ZIKV replication, protecting NES cells from cell death

Authors

Marco Onorati, Zhen Li, Fuchen Liu, ..., Tamas L. Horvath, Brett D. Lindenbach, Nenad Sestan

Correspondence

tamas.horvath@yale.edu (T.L.H.), brett.lindenbach@yale.edu (B.D.L.), nenad.sestan@yale.edu (N.S.)

In Brief

Onorati et al. establish neuroepithelial stem (NES) cells as a model for studying human neurodevelopment and ZIKV-induced microcephaly. Together with analyses in human brain slices and microcephalic human fetal tissue, they find that ZIKV predominantly infects NES and radial glial cells, reveal a pivotal role for pTBK1, and find that nucleoside analogs inhibit ZIKV replication, protecting NES cells from cell death.

Accession Numbers

GSE81475
KX197192

Onorati et al., 2016, Cell Reports *16*, 2576–2592
September 6, 2016
http://dx.doi.org/10.1016/j.celrep.2016.08.038

OPEN ACCESS
CellPress

Cell Reports
Article

Zika Virus Disrupts Phospho-TBK1 Localization and Mitosis in Human Neuroepithelial Stem Cells and Radial Glia

Marco Onorati,[1,14] Zhen Li,[1,14] Fuchen Liu,[1,14] André M.M. Sousa,[1,14] Naoki Nakagawa,[2] Mingfeng Li,[1] Maria Teresa Dell'Anno,[3] Forrest O. Gulden,[1] Sirisha Pochareddy,[1] Andrew T.N. Tebbenkamp,[1] Wenqi Han,[1] Mihovil Pletikos,[1] Tianliuyun Gao,[1] Ying Zhu,[1] Candace Bichsel,[1] Luis Varela,[4] Klara Szigeti-Buck,[4] Steven Lisgo,[5] Yalan Zhang,[6] Anze Testen,[2] Xiao-Bing Gao,[4] Jernej Mlakar,[7] Mara Popovic,[7] Marie Flamand,[8] Stephen M. Strittmatter,[3] Leonard K. Kaczmarek,[6,9] E.S. Anton,[2] Tamas L. Horvath,[1,4,10,11,*] Brett D. Lindenbach,[12,*] and Nenad Sestan[1,3,4,13,15,*]

[1]Department of Neuroscience and Kavli Institute for Neuroscience, Yale School of Medicine, New Haven, CT 06510, USA
[2]UNC Neuroscience Center and the Department of Cell Biology and Physiology, University of North Carolina School of Medicine, Chapel Hill, NC 27599, USA
[3]Cellular Neuroscience, Neurodegeneration and Repair Program, Departments of Neurology and Neuroscience, Yale School of Medicine, New Haven, CT 06510, USA
[4]Section of Comparative Medicine, Yale School of Medicine, New Haven, CT 06510, USA
[5]Institute of Genetic Medicine, Newcastle University, Newcastle upon Tyne NE13BZ, UK
[6]Department of Pharmacology, Yale School of Medicine, New Haven, CT 06510, USA
[7]Institute of Pathology, Faculty of Medicine, University of Ljubljana, Ljubljana 1000, Slovenia
[8]Department of Virology, Institut Pasteur, 75724 Paris Cedex 15, France
[9]Department of Cellular and Molecular Physiology, Yale School of Medicine, New Haven, CT 06510, USA
[10]Department of Obstetrics, Gynecology, and Reproductive Sciences, Yale School of Medicine, New Haven, CT 06510, USA
[11]Yale Program in Integrative Cell Signaling and Neurobiology of Metabolism, Yale School of Medicine, New Haven, CT 06510, USA
[12]Department of Microbial Pathogenesis, Yale School of Medicine, New Haven, CT 06510, USA
[13]Departments of Genetics and Psychiatry, Yale School of Medicine, New Haven, CT 06510, USA
[14]Co-first author
[15]Lead Contact
*Correspondence: tamas.horvath@yale.edu (T.L.H.), brett.lindenbach@yale.edu (B.D.L.), nenad.sestan@yale.edu (N.S.)
http://dx.doi.org/10.1016/j.celrep.2016.08.038

SUMMARY

The mechanisms underlying Zika virus (ZIKV)-related microcephaly and other neurodevelopment defects remain poorly understood. Here, we describe the derivation and characterization, including single-cell RNA-seq, of neocortical and spinal cord neuroepithelial stem (NES) cells to model early human neurodevelopment and ZIKV-related neuropathogenesis. By analyzing human NES cells, organotypic fetal brain slices, and a ZIKV-infected micrencephalic brain, we show that ZIKV infects both neocortical and spinal NES cells as well as their fetal homolog, radial glial cells (RGCs), causing disrupted mitoses, supernumerary centrosomes, structural disorganization, and cell death. ZIKV infection of NES cells and RGCs causes centrosomal depletion and mitochondrial sequestration of phospho-TBK1 during mitosis. We also found that nucleoside analogs inhibit ZIKV replication in NES cells, protecting them from ZIKV-induced pTBK1 relocalization and cell death. We established a model system of human neural stem cells to reveal cellular and molecular mechanisms underlying neurodevelopmental defects associated with ZIKV infection and its potential treatment.

INTRODUCTION

The human CNS is a complex organ that, as a result of its extended development, is susceptible to a host of genetic and environmental insults. Although great strides have been made in mapping the genetic landscape of human neurodevelopmental malformations, understanding of the mechanisms by which diverse environmental pathogens affect human neurodevelopment has been lagging (Bae et al., 2015; Diaz and Gleeson, 2009; Lui et al., 2011; Silbereis et al., 2016; Woods, 2004).

The emerging link between the mosquito-borne flavivirus Zika virus (ZIKV) infection of pregnant women and fetal microcephaly reinforces the need to use tissue- and species-relevant cellular systems to study human CNS development and establish experimental systems for modeling ZIKV infection, neurotropism, and treatment (Miner and Diamond, 2016; Schuler-Faccini et al., 2016). In adults, rare complications of ZIKV infection include Guillain-Barré syndrome (Broutet et al., 2016; Oehler et al., 2014) and meningoencephalitis (Araujo et al., 2016). More prominently, ZIKV infection during pregnancy is associated with, and likely causative for, severe fetal abnormalities including microcephaly/micrencephaly, lissencephaly, hydrocephaly, necrosis, periventricular and cortical calcifications, diffuse astrogliosis, hypoplasia of the brain stem and spinal cord (SC), Wallerian degeneration of the corticospinal tract, and ocular abnormalities (Brasil et al., 2016; Mlakar et al., 2016; de Paula Freitas et al., 2016; Rubin et al., 2016). More broadly, the classical teratogenic

TORCH syndrome pathogens (toxoplasma, other agents, rubella virus, cytomegalovirus, and herpes simplex virus) result in up to half of all perinatal deaths around the world, many associated with brain malformations including microcephaly, with an especially large burden in developing countries (Adams Waldorf and McAdams, 2013; Fine and Arndt, 1985).

Primary microcephaly results mainly from the depletion of neural stem/progenitor cells due to centrosomal defects, premature differentiation, and/or cell death (Diaz and Gleeson, 2009; Woods, 2004). Recently, ZIKV was shown to preferentially infect human pluripotent stem cell (hPSC)-derived neural progenitors and organoids and cause mitotic impairment and cell death in ZIKV mouse models (Dang et al., 2016; Garcez et al., 2016; Qian et al., 2016; Tang et al., 2016; Lazear et al., 2016; Li et al., 2016; Cugola et al., 2016; Miner et al., 2016; Wu et al., 2016). However, the human CNS is distinct in the diversity and proliferative potential of neural stem and progenitor cells (Lui et al., 2011; Bae et al., 2015; Silbereis et al., 2016; Gage and Temple, 2013). As a result, there may be aspects of viral infection that are unique to the human brain. Moreover, there have been only limited reports to date on human cell-type-specific responses to ZIKV over the course of infection primarily in in vitro or murine model systems without comparison to infected human brain tissue. Finally, it is not known to what extent microcephaly results from direct ZIKV infection of developing neural cells versus indirect effects, such as inflammation and altered placental support, which has been shown to affect brain development (Burton and Fowden, 2015; Mor, 2016). Addressing these questions in the context of the developing human CNS is crucial for deciphering ZIKV tropism and neuropathogenesis.

Here, we describe the derivation and characterization of neocortical (NCX) and SC neuroepithelial stem (NES) cells as in vitro models for neural stem/progenitor cells, early human neurodevelopment, and ZIKV-related neuropathogenesis. NES cell lines are derived from primary neuroepithelial cells, the earliest population of resident neural stem cells present during neurodevelopment, when the neural tube is comprised of a pseudostratified neuroepithelium lining the central cavity (Bae et al., 2015). These cells constitute the ventricular zone (VZ) of the neural tube and serve as the stem cells of the CNS. Initially, neuroepithelial cells divide symmetrically in order to expand the stem cell pool (Silbereis et al., 2016). Later on, neuroepithelial cells transition into radial glia cells (RGCs), which reside in the VZ and inner (iSVZ) and outer subventricular zone (oSVZ). These cell populations serve as the stem or progenitor cells for neurons and macroglia (i.e., astrocytes and oligodendrocytes) and provide scaffolding for migrating nascent neurons (Bae et al., 2015). RGCs largely divide asymmetrically, giving rise to a daughter RGC, an intermediate progenitor cell (IPC), or a nascent neuron that subsequently migrates. Because of the ability to self-renew and differentiate, neuroepithelial cells are ideal candidates for the study of neural stem cell biology and various developmental diseases.

By comparing NES cells, organotypic fetal brain slices, and the postmortem human tissue in the context of ZIKV infection, we show that ZIKV infects both NCX- and SC-NES cells and their fetal homolog, RGCs in the VZ and SVZ, and to a lesser extent, postmigratory neurons in the cortical plate (CP; anlage of the cerebral cortical layers 2–6). ZIKV infection is associated with mitotic impairment, structural disorganization of the proliferative zones, and increased cell death of NES cells and RGCs. We also found that ZIKV causes subcellular relocation of the phosphorylated TANK binding kinase 1 (pTBK1), a pivotal player in antiviral innate immunity and cell proliferation (Farlik et al., 2012; Helgason et al., 2013; Pillai et al., 2015; Thurston et al., 2009) from centrosomes to mitochondria during mitosis of NES cells and RGCs. Antiviral nucleoside analogs, including the FDA-approved drug Sofosbuvir, inhibit ZIKV replication and ZIKV-induced cytopathology, including the relocalization of pTBK1 to mitochondria, in NES cells. Together, these results validate the use of this NES cell system as an experimental model for studying early human neurodevelopment and ZIKV-induced pathogenesis, provide a testable hypothesis for the mechanism of ZIKV-induced cytopathology, and lay the groundwork for future research on ZIKV-related neurodevelopmental defects and therapy.

RESULTS

Derivation of Human Neocortical and Spinal Cord Neuroepithelial Stem Cells

Different early human neural stem/progenitor cell types, including neuroepithelial-like cells, have been derived from hPSCs and the developing human brain (Conti and Cattaneo, 2010; Edri et al., 2015; Elkabetz et al., 2008; Sun et al., 2008, Tailor et al., 2013). However, stable cell lines of neuroepithelial cells have not been derived from the dorsal forebrain (prospective NCX) or the SC. Thus, we attempted to generate stable long-term, self-renewing populations of NCX and SC neuroepithelial cells from ten human specimens ranging from 5 to 8 postconceptional weeks (pcw; Carnegie stage 15–17) (Figure 1A and Table S1).

Dissociated cells were plated and examined for the presence of neural rosettes reminiscent of the radial arrangement and apico-basal polarization established by neuroepithelial cells in the native neural tube (Figure 1B). In total, we derived and characterized five stable NCX and three stable SC neuroepithelial cell lines. Moreover, after propagation in the presence of the growth factors FGF2 and EGF as well as BDNF (Figures S1A and S1J), the neuroepithelial cell lines exhibited stem/progenitor cell characteristics and retained a high neurogenic capacity; thus, we termed them NCX- and SC-NES cells, respectively. Both NCX- and SC-NES cells were immunopositive for the neuroepithelial marker SOX1 and the pan-neural stem cell markers nestin, SOX2, and vimentin (VIM) (Figures 1C, 1D, S1B, and S1K). Metaphase NES cells were also observed and labeled with the anti-phospho-VIM antibody, and some displayed a typical basal process (Figure S1C).

Next, we investigated whether NES cells retained regional identity after long-term expansion. NCX-NES cells expressed FOXG1 and OTX2 (Figures 1E and S1D), key transcription factors demarcating proliferative zones of the early human forebrain (Onorati et al., 2014). On the other hand, SC-NES cells were positive for the caudal regional marker HOXB4 (Krumlauf et al., 1993) (Figure S1L), thus demonstrating maintenance of regional identity even after more than ten passages. These cell lines have

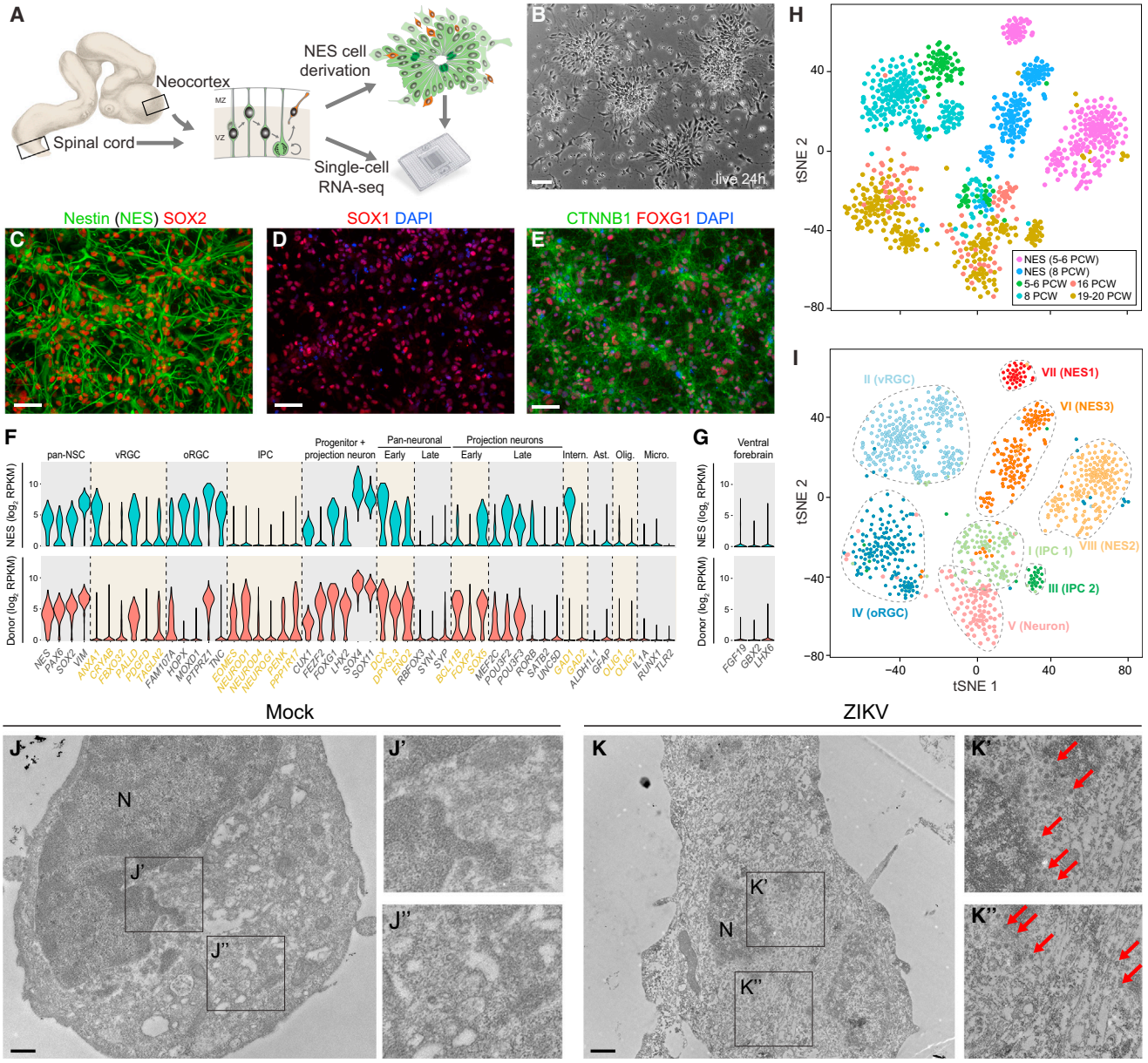

Figure 1. Derivation, Profiling, and ZIKV infection of NES Cells

(A) A schematic of experimental procedure. NES cells were derived from human developing neocortex (NCX) or spinal cord (SC). Donor-matched brain tissues and NCX-NES cells were subjected to single-cell RNA-seq. SC-NES cells are described in Figure S1.

(B) NCX-NES cells form rosette structures after 24 hr in culture. Scale bars represent 50 μm.

(C–E) NCX-NES cells are positive for nestin (NES), SOX2 (99.4% ± 0.8%, n = 973), SOX1 (87.8% ± 1.9%, n = 1265), CTNNB1, and FOXG1 (96.5% ± 1.1%, n = 1277). Scale bars represent 50 μm. Results are presented as mean ± SD.

(F) Violin plots showing expression of cell-type-specific marker genes in NCX-NES cells and donor-matched NCX tissue single cells. pan-NSC, pan-neural stem cell; vRGC, ventricular radial glia cell; oRGC outer radial glia cell; IPC, intermediate progenitor cell; Intern., interneuron; Ast., astrocyte; Olig., oligodendrocyte; Micro., microglia. y axis, $\log_2$ transformed RPKM.

(G) As in (F), violin plots of ventral forebrain marker genes in NCX-NES and donor-matched NCX single cells.

(H and I) t-SNE plots of all NES cell lines and brain single cells colored by origin of the cells (H) or by cell type clusters identified with SNN-Cliq clustering algorithm (I).

(J and K) Electron microscopy images of mock (J) or ZIKV-infected (K) NCX-NES cells. Nucleus (N) appears to be normal (J'), and cytoplasm is clear of ZIKV viral particles (J'') in mock condition. Nuclear fragmentation is evident in the ZIKV-infected condition. Viral particles are evident around nuclear envelope (red arrows in K', K''). Scale bars represent 1 μm.

See also Figures S1–S4.

been expanded for more than 1 year and 35 passages with no evidence of chromosomal instability (Figures S1E and S1M).

To test the neurogenic potential of NES cells, we used an optimized differentiation protocol (Figure S1F). All NES cells gave rise to MAP2$^+$ and TUBB3$^+$ neurons and extended neurites (Figures S1G and S1H). We found that NCX-NES cells differentiated into neurons positive for BCL11B (also known as CTIP2), a marker of deep-layer excitatory projection neurons in the NCX (Figure S1H). SC-NES cells also gave rise to TUBB3-, MAP2-, and RBFOX3 (also known as NeuN)-positive neurons, whereas some exhibited a cholinergic phenotype, as expected for a SC neuronal population (Figures S1N and S1O). Furthermore, GFAP$^+$ astroglial cells (Figures S1I and S1P) and occasional O4$^+$ oligodendrocytes were detected (Figure S1Q), thus demonstrating the multipotential stem cell capacity of NES cells.

Human NES Cells Exhibit the Transcriptional Signature of Early Neural Stem Cells

To further characterize NCX-NES cells, we conducted single-cell RNA-seq on 439 expanded NCX-NES cells and 383 cells from 5–6 and 8 pcw donor-matched NCX (Tables S1 and S2); 362 and 255 cells, respectively, passed our quality-control pipeline (Supplemental Experimental Procedures). The majority of cells analyzed from the donor-matched NCX tissue samples expressed canonical marker genes for neuroepithelial cells and RGCs of the dorsal forebrain (Figure 1F). NCX-NES cells showed similar expression profiles as their donor-matched NCX cells (Figure 1F). Neither brain NCX cells nor NCX-NES cells expressed ventral forebrain markers (Figures 1G and S2D).

To place the transcriptional profiles of NCX-NES cells within the context of fetal development, we supplemented our donor-matched datasets with single-cell RNA-seq data from 526 cells collected from fetal NCX at 16, 19, and 20 pcw (Figure 1H); 392 of them passed quality control. We conducted principal component analysis for dimension reduction with genes as observations and single cells as variables (Figure S2A). The first principal component was used as the representation of each fetal time point or NCX-NES cell line. Pairwise Pearson's correlation test showed that NCX-NES cells highly correlated with embryonic development time points ($r > 0.8$; Figure S2B). We next applied a clustering algorithm designed for single-cell studies, SNN-Cliq, to explore cellular composition over neocortical development and in NCX-NES cells. Based on the expression of marker genes for various cell types, we identified five NCX clusters (Figure S2C) representing ventricular and outer RGCs (vRGCs and oRGCs, respectively), two types of IPCs, and early neurons (Figure 1I). As expected from the expression profiles of NCX-NES cells, the largest of the three NCX-NES cell clusters highly correlated with the vRGC and IPC clusters, while the other two NCX-NES cell clusters showed neuroprogenitor-like gene expression profiles (Figure S2D). Together, these data establish NES cell lines as relevant models of early human CNS development.

Human NES Cells, but Not NES-Derived Neurons, Can Be Efficiently Infected by ZIKV

We sought to test whether the NCX-NES cell system can be used as a model for ZIKV infection. First, we infected NCX-NES cells with the 2010 Cambodian ZIKV strain FSS 13025 (MOI = 0.1), which shares 98% nucleotide identity with the current Brazilian epidemic strain. We monitored NCX-NES cells up to 6.5 days post-infection (DPI). At 3.5 DPI, we observed widespread ZIKV infection, as demonstrated by immunolabeling for the viral nonstructural protein 1 (NS1), with over 90% of NCX-NES cells infected (Figures S3A and S4F). We also observed a significant decrease in cell density over time compared to mock-infected cells (Figure S3B). Notably, the number of active caspase 3 (aCASP3$^+$) apoptotic cells as well as pyknotic cells (i.e., cells showing condensation of the chromatin) was significantly higher in the infected group at 3.5 and 6.5 DPI compared to mock control (Figures S3C and S3D). Based on the analysis of immunolabeling for MKI67 (also known as Ki-67), a static marker of proliferative activity, we found that the proliferation levels were also significantly decreased by 3.5 DPI, with a continued decline through 6.5 DPI (Figures S3E and S3F). Electron microscopy also showed viral particles in infected NCX-NES cells and signs of nuclear fragmentation compared to mock cells (Figures 1J and 1K).

Recent studies have shown that hPSC-derived and mouse neural progenitors and neurons are infected by ZIKV, though neural stem and progenitor cells are preferential targets of infection (Qian et al., 2016; Tang et al., 2016). To test this in our model system, ZIKV was used to infect NCX-NES cells after differentiating them into neurons for 48 days. At 3.5 DPI, no obvious increase in the cytopathic effect or cell death was evident in the ZIKV-treated cultures (Figures S4A and S4B). In order to discriminate between ZIKV infection of neurons, which are postmitotic and express high levels of MAP2, and progenitors, we administered 5-bromo-2′-deoxyuridine (BrdU), a thymidine analog that incorporates into newly synthesized DNA, before ZIKV infection (Figure S4C). We found that only ~7.2% of the cells in the neuronal cultures were NS1$^+$ (Figures S4D, S4E, and S4F). Among the NS1$^+$ neurons, 46% were BrdU$^-$, thus indicating that only ~3.3% of postmitotic neurons were infected by ZIKV (Figures S4G, S4H, and S4I). Therefore, the ability of ZIKV to infect neurons is extremely low in comparison to its ability to infect self-renewing NES cells (~90%, Figure S4F). This result also suggests that some NES cells infected during mitosis could have passed the infection onto daughter cells destined to become neurons.

ZIKV Preferentially Infects RGCs, Causing Scaffold Disorganization in Fetal Organotypic Slices

In addition to NES cells, we also infected ex vivo human organotypic fetal brain slices with ZIKV strain FSS 13025 (Figure 2A and Table S3). Before infection, brain slice cultures showed completely normal anatomical structures of the developing NCX, including an intact VZ/SVZ, intermediate zone/subplate (IZ/SP) and CP, with a prominent RG scaffold (Figure 2B). At 1.5 DPI, only a few cells were infected, and nearly all infected cells resided in the VZ/SVZ (Figure 2C); no obvious anatomical or cellular defects were otherwise observed. Interestingly, we did not observe any postmigratory neurons in the CP that were NS1$^+$ at 1.5 DPI (Figure 2C). A dramatic increase in the number of NS1$^+$ cells was evident at 3.5 and 6.5 DPI, mostly located in the VZ, SVZ, and IZ/SP (Figures 2F and 2G). A majority

of NS1-expressing cells also stained positive for the RGC marker VIM (Figures 2C, 2F, and 2G). Immunostaining of VIM showed that the RG scaffold was disorganized and that the radial organization of neurons in the CP was altered adjacent to highly infected regions of brain slices as compared to less infected regions or uninfected control (Figures 2D, 2E, 2F, and 2G). By 6.5 DPI, architectural disorganization was even more pronounced, with non-infected VIM$^+$ RGCs acquiring a ''balloon'' shape, suggesting an indirect, non-cell-autonomous effect of ZIKV-infected cells (Figures 2F and 2G).

To test whether ZIKV-induced effects are virus strain specific, we tested the neurotropism of a Brazilian ZIKV strain, PE243, on NES cells, revealing an extensive NS1-positivity at 3.5 DPI (Figure S5A), which was not present in mock-infected cells or cells exposed to UV- or low pH-inactivated ZIKV particles. ZIKV PE243 also infected a neural primary culture from a 15 pcw NCX tissue, with a widespread NS1$^+$ signal (Figure S5B). ZIKV PE243-infected organotypic brain slices also exhibited an architectural disorganization of the RG scaffold at 3.5 DPI. (Figure S5C).

Neocortical RGCs Contain ZIKV in an Infected Human Microcephalic Fetus

To confirm that ZIKV infection of RGCs is linked with microcephaly/micrencephaly, we examined postmortem forebrain and SC tissues of the first reported ZIKV-infected microcephalic fetus (approximately 30 pcw, Table S4) from a ZIKV-infected mother (Mlakar et al., 2016) (Figure 3A). ZIKV RNA was previously found in the brain tissue of this fetus by RT-PCR (Mlakar et al., 2016). Tissue sections of the forebrain were immunopositive for NS1 and the ZIKV envelope (E) glycoprotein in the neocortical VZ and SVZ RGCs (Figures 3B–3E), which were identified by their position, morphology and the expression of VIM (Figures 3G and 3I). Regions of the neocortical VZ/SVZ and RG morphology in those regions were disorganized in the infected brain, with numerous ventricular protrusions and a visually apparent decrease in the density of basal processes from RGCs as compared to an age-matched postmortem control (Figures 3F and 3H). RGCs also clustered abnormally in the VZ/SVZ, and the RG scaffold was disorganized, particularly in aCASP3$^+$ cells, as indicated by nestin or VIM staining (Figures 3I, 3L, and 3M). Neurons in the NCX appeared disorganized and dysplastic, which could be due to either direct infection by ZIKV or indirectly through altered migration and neuron placement resulting from disruptions to the RG scaffold (Figure 3J). We did not observe infected cells in the ependymal layer, derivatives of RGCs lining the central canal of the SC (Figure 3K).

NES Cells and RGCs Express the Putative ZIKV Entry Receptors AXL and TYRO3

To better understand why ZIKV preferentially infects neural stem cells and RGCs, we surveyed the expression of putative ZIKV entry receptors in the NCX-NES cells and human fetal brain. Recent studies suggested that a number of cell-surface proteins may serve as ZIKV entry factors, including AXL, TYRO3, CD209, HAVCR1, and TIMD4, with AXL being the most plausible candidate (Hamel et al., 2015; Nowakowski et al., 2016). Among these five putative receptors, single-cell RNA-seq analysis found that *AXL* was generally expressed at the highest and most consistent levels in NCX-NES cells and RGCs and IPCs from the developing NCX (Figure 4A), whereas *TYRO3* was expressed inconsistently and other receptors were essentially not expressed by NES cells, RGCs, and IPCs (Figures 4A and S2D). Analysis of previously published adult single-cell sequencing data (Darmanis et al., 2015) indicated that *AXL* was highly expressed in adult astrocytes, microglia, and endothelial cells but not in neurons (Figures 4B and S6A). Analysis of tissue-level transcriptome data from the developing human brain (Kang et al., 2011) showed that both *AXL* and *TYRO3* expression in the NCX have bimodal patterns, with high expression in embryonic and early fetal samples and again increased expression beginning during late fetal development that remains at elevated levels after birth until adulthood (Figures 4C and 4D), which was consistent with the pattern of astrocyte generation (Zhang et al., 2016).

We corroborated the transcriptional data through immunofluorescence analysis of AXL protein expression and found co-expression of AXL and VIM in NCX-NES cells (Figures 4E and 4F). AXL expression in 14 pcw NCX was detected in VZ and VIM$^+$ RGC basal processes as well as in blood vessels (Figure 4G). AXL was highly expressed in the VZ/SVZ but not the CP of fetal organotypic slice cultures (Figure 4H). Interestingly, NS1 staining was close to AXL staining in infected organotypic slices (Figure 4H). AXL signal was scarcely detectable in adult neocortical astrocytes, restricted to their end-feet contacting blood vessels, and in the periventricular astrocyte ribbon (Figure 4I). Taken together, these observations support AXL and possibly TYRO3 as viral entry factors and may explain the cell-type specificity of ZIKV infection in NES cells and RGCs (Nowakowski et al., 2016).

ZIKV Infection Redirects pTBK1 from Cytoplasm and Centrosomes to Mitochondria during Mitosis

Recent work reported that ZIKV disrupts mitosis and increases cell death in neural stem cells (Garcez et al., 2016; Qian et al., 2016), although the molecular basis of these effects is unknown. TANK-binding kinase 1 (TBK1) is a cellular serine-threonine kinase that is essential for both innate antiviral immune signaling and for cell proliferation as well as other processes (Farlik et al., 2012; Helgason et al., 2013; Pillai et al., 2015; Thurston et al., 2009). We hypothesized that ZIKV could disrupt NES cell proliferation by diverting TBK1 activity away from mitosis and toward innate immune signaling. By using single-cell RNA-seq data, we found that *TBK1* was highly expressed in both NES cells and RGCs/IPCs in the fetal NCX but not in immature neurons (Figure 5A). Single-cell RNA-seq data also showed that *TBK1* is highly expressed in neurons, astrocytes, and microglia in the adult brain (Figure 5A). Consistent with this expression, analysis of a developing human brain transcriptome dataset (Kang et al., 2011) revealed a bimodal pattern of *TBK1* expression in the NCX, with high expression in the embryonic and early fetal samples and again during postnatal development (Figure S6B).

To investigate whether *TBK1* levels changed during ZIKV infection, we conducted droplet digital PCR (ddPCR) on both ZIKV-infected and mock-infected NES cells and organotypic brain slices. No differences in *TBK1* levels were found between uninfected and ZIKV-infected (with either the Cambodian or

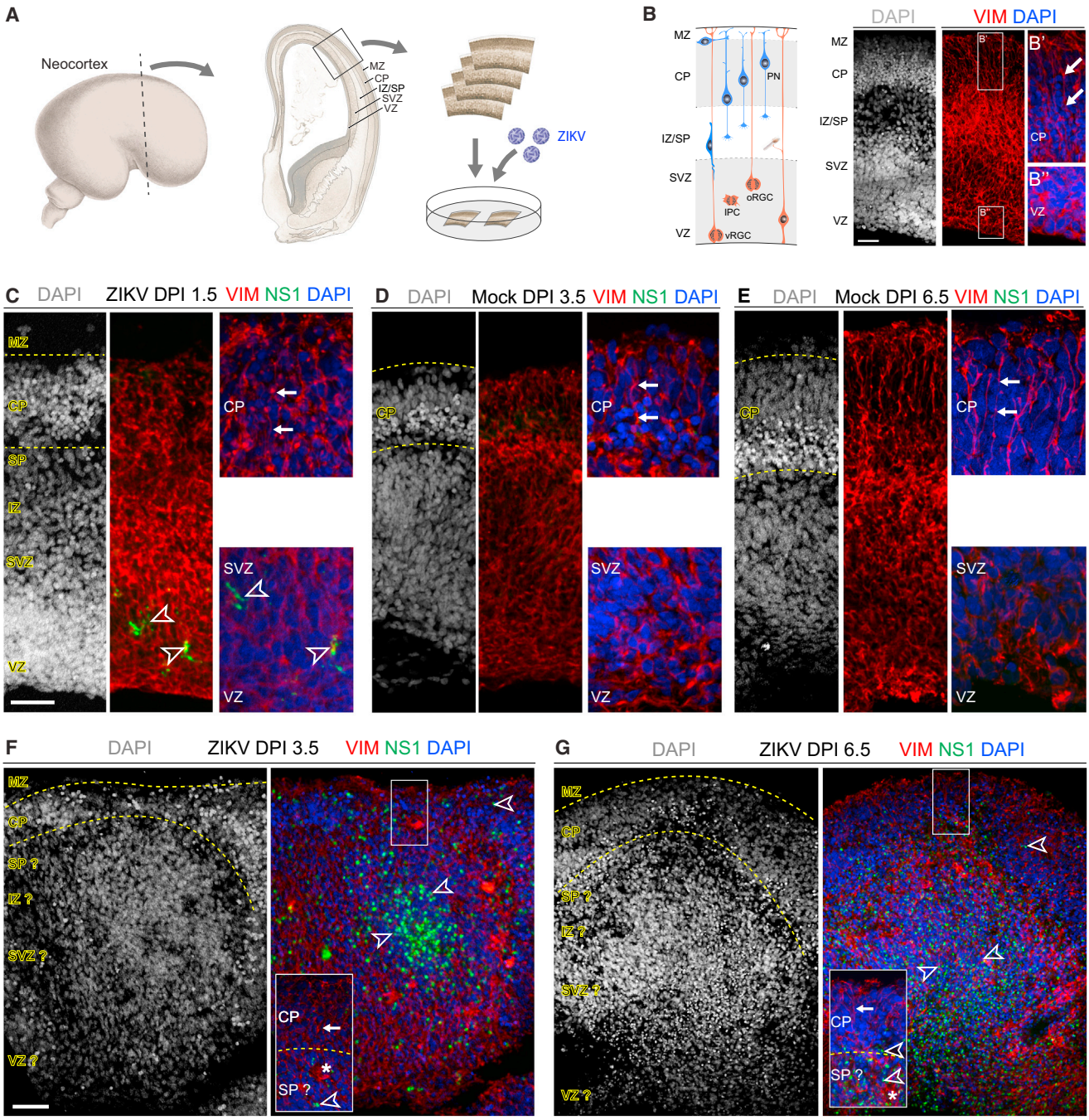

Figure 2. ZIKV Infects RGCs and Disrupts RG Scaffolding of Fetal Neocortical Organotypic Slices

(A) A schematic representation of the experimental procedure.

(B) Schematic illustration of the early fetal NCX. Vimentin (VIM) and DAPI immunostaining of pre-infection slices shows a normal architecture of neocortical wall. Higher magnification of CP and VZ reveals the radial organization of VIM$^+$ RG fibers reaching the pial surface. MZ, marginal zone; CP, cortical plate; IZ/SP, intermediate zone/subplate; SVZ, subventricular zone; VZ, ventricular zone; PN, projection neuron; oRGC, outer radial glia cell; IPC, intermediate progenitor cell; vRGC, ventricular radial glia cell.

(C) Organotypic brain slices show ZIKV infection in RGCs at 1.5 days post infection (DPI); 80.6% ± 0.6% of the infected cells localized in VZ/SVZ, 19.4% ± 4% in the IZ/SP, and none in CP (total number of infected cells = 20). VZ/SVZ are significantly more infected than CP (paired t test, $p < 0.05$). The slices maintain a normal structure, with radial glial fibers reaching the pial surface and a normal orientation in VZ and SVZ.

(D and E) Non-infected neocortical slices show normal morphology and RG scaffold at both 3.5 (D) and 6.5 (E) DPI.

(F and G) ZIKV-infected slices show severe defects in RG scaffolding at 3.5 (F) and 6.5 (G) DPI. Most of the infected cells are located in VZ/SVZ and IZ/SP regions (73.3% ± 28.7% at 3.5 DPI; 89.3% ± 3.4% at 6.5 DPI), with fewer CP neurons showing infection (26.7% ± 28.7% at 3.5 DPI and 10.7% ± 3.4% at 6.5 DPI,

(legend continued on next page)

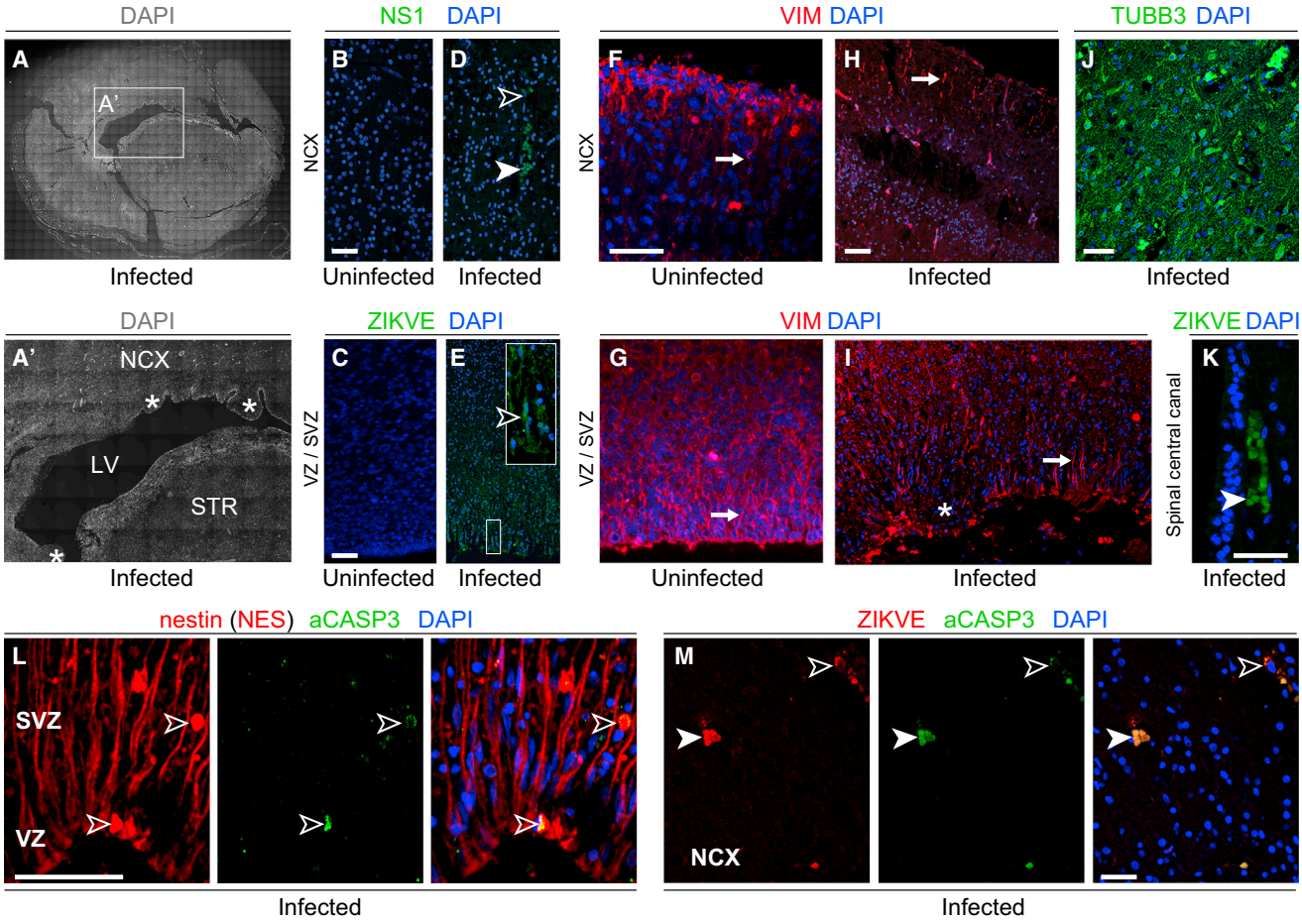

Figure 3. Neocortical RGCs Express ZIKV Epitopes in a Late Fetal Microcephalic ZIKV-Infected Brain

(A) Tissue section of a 30 pcw microcephalic fetus from a ZIKV-infected mother. Higher magnification shows protrusions (asterisk) in ventricular zone (VZ) (A'). LV, lateral ventricle; STR, striatum; NCX, neocortex.

(B and C) Immunostaining of an uninfected brain show no NS1$^+$ cells in NCX (B) and no ZIKVE$^+$ cells in the NCX VZ/SVZ (C).

(D and E) In the infected brain, most of the infected cells (arrowhead) are in VZ/SVZ (64.2% of the total cells) (D). Only 1.2% of CP cells are ZIKV-infected (D) (number of total analyzed cells in the single microcephalic fetal human brain reported = 1,050). Filled arrowheads depict red blood cells (D).

(F and G) Immunostaining for vimentin (VIM) in both VZ/SVZ, and NCX shows a normal radial orientation of basal processes of RGCs (arrow).

(H) Upper layers of the NCX show an impaired organization and lower nuclei density in comparison to uninfected control NCX. Arrow depicts a defective radial process.

(I) Periventricular region showing dysplastic intraventricular protrusions with lower density of RGCs (asterisk) and disorganized RG morphology (arrow) and processes.

(J) NCX of the infected brain displays disorganized arrangement of dysplastic TUBB3$^+$ neurons.

(K) Central canal of the SC immunostained for ZIKVE. Filled arrowhead shows positive red blood cells. Ependymal cells are not labeled.

(L) Co-labeling of nestin (NES) and aCASP3 shows positive cells (arrowheads) in the infected brain with no radial fibers.

(M) ZIKVE and aCASP3 staining shows positive cells (arrowheads) in the infected NCX. Filled arrowheads depict red blood cells.

Scale bars represent 50 μm.

Brazilian ZIKV strains) NES cells or organotypic slices, though expression of *TBK1* in the relatively homogeneous NES cell population was greater than in the organotypic brain slices, which are composed of both neural stem/progenitor cells and immature postmitotic neurons (Figure 5B). This indicates that ZIKV infection does not lead to obvious changes in *TBK1* mRNA

respectively; total number of infected cells = 456 at 3.5 DPI and 1,315 at 6.5 DPI). At 6.5 DPI, CP was significantly less infected than the other zones of the NCX (paired two-tailed t test, $p < 0.01$). Regions with high numbers of infected cells (shown in between arrowheads) show a more pronounced defect in radial orientation of RG fibers. Furthermore, it is possible to observe balloon-like cells that express VIM.

Arrowheads indicate cells that are infected with ZIKV, immunopositive for NS1. Arrows show RG fibers. Scale bars represent 50 μm. Results are presented as mean ± SD.

See also Figure S5.

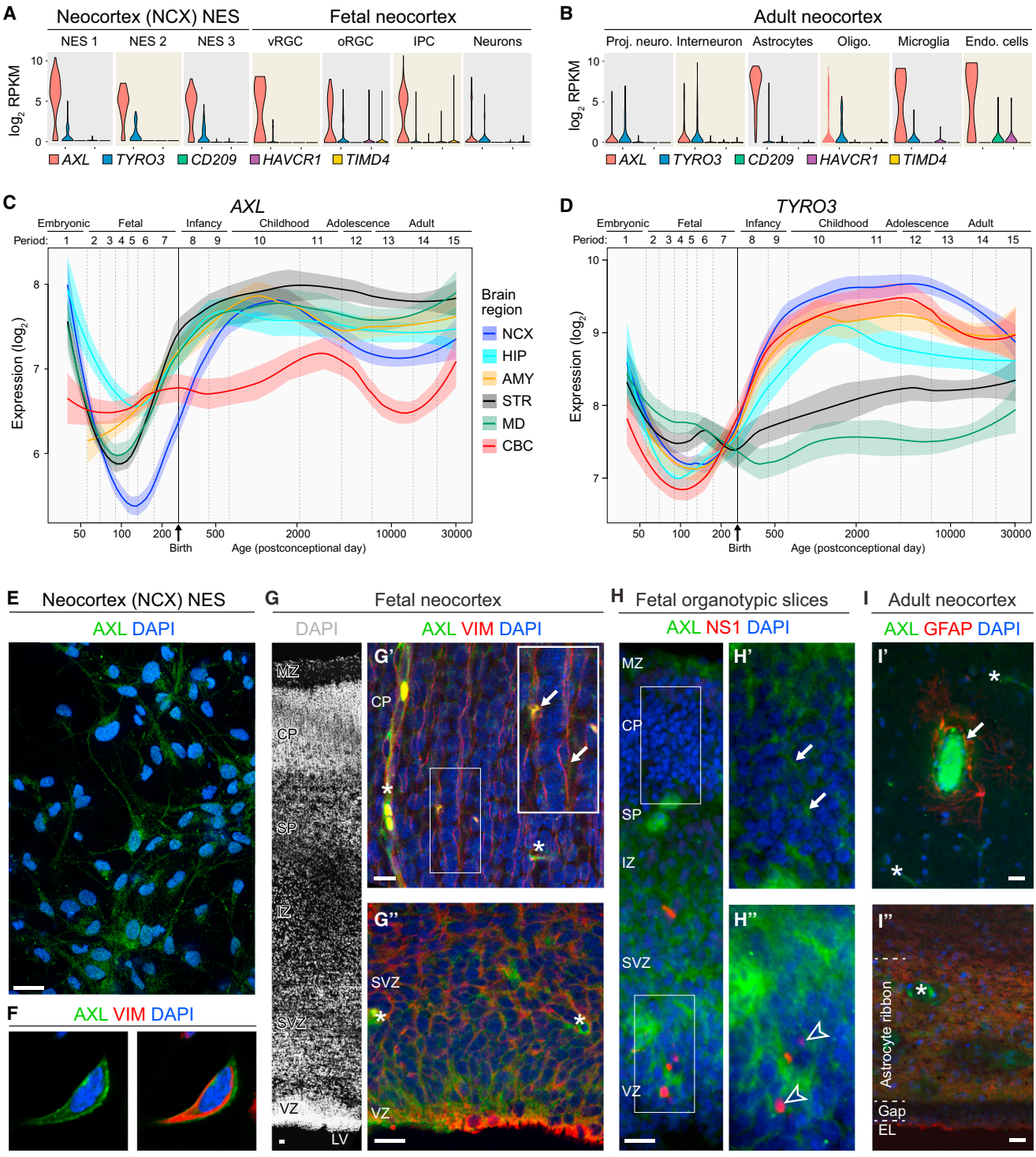

Figure 4. NES Cells and RGCs Express Candidate ZIKV Entry Receptors *AXL* and *TYRO3*

(A and B) Violin plots of candidate entry factor gene expression distributions in NCX-NES and donor-matched NCX single cells (A) or adult NCX (B). y axis, $\log_2$ transformed RPKM (A) or $\log_2$ transformed RPM (B). Proj. neuro., projection neuron; Interneuro., interneuron; Oligo., oligodendrocyte; Endo. cells, endothelial cells.

(C and D) Expression trajectories of *AXL* (C) and *TYRO3* (D) during human neurodevelopment in different brain regions. y axis represents gene expression quantified by $\log_2$ transformed signal intensities and the x axis represents the developmental ages quantified by the $\log_{10}$ transformed postconceptional days.

(legend continued on next page)

expression in our two model systems. We therefore surveyed protein expression by immunoblotting for TBK1 and phosphorylated TBK1 (pTBK1) on human tissue from fetal VZ/SVZ and CP and found that there was a higher level of pTBK1 in VZ/SVZ compared to CP (Figure 5C). Furthermore, immunofluorescence analysis revealed that phospho-VIM$^+$ mitotic NES cells co-expressed pTBK1 in centrosomes and midbody (Figure 5D). Consistent with this, pTBK1$^+$ cells co-expressed PAX6 in the VZ/oSVZ of the fetal neocortical wall (Figure 5D). Together, these results suggest that ZIKV affects the localization or activity of TBK1 without substantially altering *TBK1* expression.

We therefore examined the localization of pTBK1 in NCX-NES cells and organotypic slices during ZIKV infection. We found that pTBK1 localized to the centrosomes in NCX-NES cells and RGCs of organotypic brain slices, as demonstrated by co-staining of pTBK1 and TUBG (also known as γ-tubulin) (Figures 5E, 5G, 5K, and 5M). In contrast, pTBK1 was no longer detected in centrosomes in ZIKV-infected cells but was instead localized to mitochondria, as shown by colocalization with ATP5A1 (Figures 5F, 5H, 5L, 5N, and 5O). Relocalization of pTBK1 to mitochondria in ZIKV-infected NES cells was confirmed by immunoelectron microscopy (Figures 5I and 5J). ZIKV-infected cells also exhibited disrupted mitotic progression, including an increase in the number of NES cells and RGCs containing more than two centrosomes (Figures 5H, 5N, and 5P). Mitochondrial shape also appeared different, as shown by electron microscopy, with increased mitochondrial area in ZIKV-infected NES cells, whereas mitochondrial density was unchanged (Figure 5Q).

TBK1 Inhibitors Impair Mitosis, Provoke Supernumerary Centrosomes in NES Cells, and Exacerbate ZIKV-Related NES Cell Death

Given that the enrichment of pTBK1 at centrosomes of mitotic NES cells and RGCs is altered by ZIKV infection and that TBK1 has been functionally linked to mitosis (Pillai et al., 2015), we asked whether pharmacological inhibition of TBK1 kinase activity could mimic the impairment caused by ZIKV infection. We therefore treated NCX-NES cells with a small-molecule inhibitor of TBK1/IKKε, Amlexanox, which inhibits TBK1 activity but not its phosphorylation on Ser172 (Reilly et al., 2013). We found that Amlexanox caused a significant decrease in the number of pTBK1$^+$ mitotic cells and increased the number of cells exhibiting supernumerary centrosomes 3.5 days after application (Figures 5R and 5S). Similar effects were demonstrated by another TBK1 inhibitor, BX795 (Figures 5R and 5S). These results are consistent with our previous finding that ZIKV-induced pTBK1 relocalization correlates with the neurodevelopmental pathology seen in the infected human brain.

TBK1 also instructs autophagy and apoptosis (Helgason et al., 2013). Therefore, inhibition of TBK1 may protect cells from cell death. We next investigated whether inhibiting TBK1 kinase activity impacts ZIKV-induced death of NCX-NES cells at 3.5 DPI. Application of Amlexanox or BX795 had no effect on cell death of uninfected cells (Figures S7A and S7B). However, both inhibitors modestly but significantly increased apoptotic cell death in ZIKV-infected NCX-NES cells (Figures S7A and S7B). Next, we also tested whether the two inhibitors can affect cell death in ZIKV-infected SC-NES cells at 3.5 DPI. Surprisingly, Amlexanox modestly decreased aCASP3$^+$, whereas BX795 had no effect at 3.5 DPI (Figure S7C). We tested the effect of Amlexanox at 5.5 DPI and found that it increased aCASP3$^+$ in SC-NES cells as observed in NCX-NES cells at 3.5 DPI (Figures S7E and S7F). Together, these results suggest that inhibition of TBK1 kinase activity can lead to severe cellular defects in mitotic NES cells and thus may exacerbate ZIKV-related cytopathology.

Relocalization of pTBK1 by Other Viruses and Innate Immune Stimulation

Given that TBK1 activation is an important component of innate antiviral signaling, we examined whether infection with another flavivirus, dengue-2 virus (DENV), or the TORCH pathogen, human cytomegalovirus (HCMV), could induce similar relocalization of pTBK1. Both DENV and HCMV infected NES cell cultures (Figures 6A and 6B) but had different effects on pTBK1 localization. Although HCMV also induced mitochondrial targeting of pTBK1, DENV did not (Figures 6A and 6B). This could be because DENV is known to inhibit the transduction of cytosolic RIG-I-like receptor (RLR) signaling through mitochondrial antiviral signaling (MAVS) and TBK1 to initiate cellular innate antiviral programs (Dalrymple, Cimica, and Mackow, 2015; He et al., 2016). Nevertheless, both DENV and HCMV induced cell death via CASP3 activation (Figure 6C). These data show that TBK1 activation and mitochondrial localization of pTBK1 is not specific to ZIKV.

To determine whether RLR activation alone could induce the relocalization of pTBK1 from centrosomes to mitochondria, we treated NES cells with KIN1408, a small-molecule agonist of RLRs (Pattabhi et al., 2016). Indeed, KIN1408 treatment induced relocalization of pTBK1 from centrosomes to mitochondria (Figures 6D and 6E) and increased CASP3-mediated cell death (Figures 6D and 6F). Together, these data suggest that ZIKV may

The dash vertical lines indicate the 15 developmental periods as defined by Kang et al. (2011). The trajectory curves are smoothed by LOWESS function. The shading areas represent mean ± SEM. NCX, neocortex; HIP, hippocampus; AMY, amygdala; STR, striatum; MD, mediodorsal nucleus of the thalamus; CBC, cerebellar cortex.
(E and F) Immunostaining showing that NES cells co-express AXL and VIM.
(G) Immunostaining of AXL and VIM in a 16 pcw fetal NCX shows that AXL is predominantly lowly expressed in the CP (G'), where it is detected mainly in blood vessels. Contrarily, higher expression of AXL is detected in the VZ/SVZ (G'').
(H) Fetal organotypic slices infected with ZIKV are NS1$^+$ in VZ/SVZ RGCs that are also AXL$^+$. Arrows point to AXL$^+$ cells. Arrowheads indicate the presence of ZIKV infection. Asterisks indicate signal blood vessels.
(I) Expression of AXL in the adult NCX is restricted mainly to the astrocyte ribbon, which is also strongly labeled by GFAP, endothelial cells, and some astrocyte processes in CP.
MZ, marginal zone; CP, cortical plate; IZ, intermediate zone; SP, subplate; SVZ, subventricular zone; VZ, ventricular zone; LV, lateral ventricle; EL, ependymal layer. Scale bars represent 50 μm
See also Figure S6.

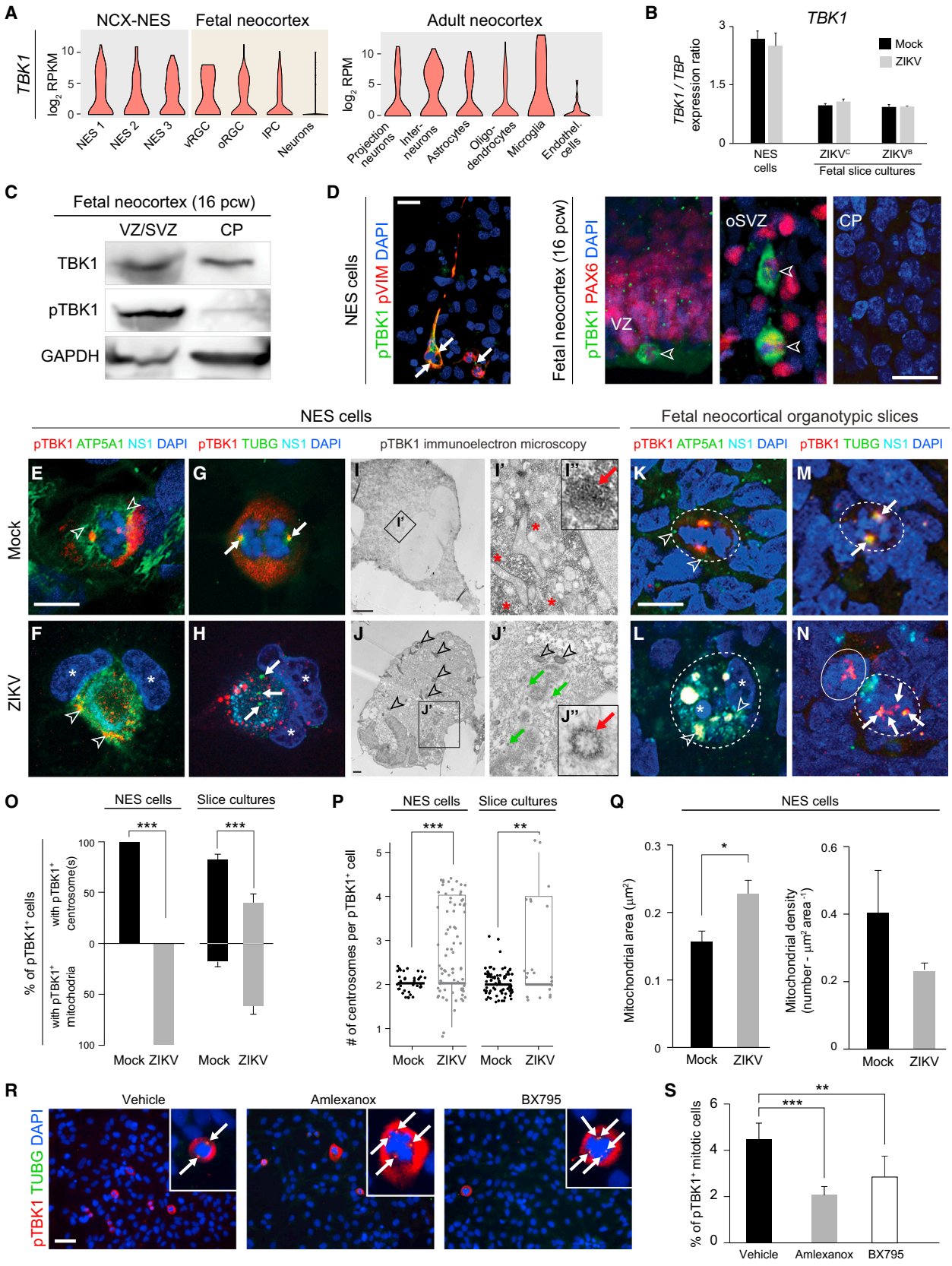

(legend on next page)

activate RLRs, causing relocalization of pTBK1 from mitotic centrosomes to mitochondria, disruption of mitosis, and induction of cell death.

Nucleoside and Nucleotide Analogs Inhibit ZIKV Replication and Protect NES Cells

There is an urgent need to identify therapeutic approaches for halting ZIKV infection, especially in pregnant women (Barrows et al., 2016). Chain-terminating nucleoside analogs have proven to be potent, broad-spectrum antivirals. Indeed, a few nucleoside analogs have already been shown to inhibit ZIKV in cell culture and mouse models of infection (Zmurko et al., 2016; Eyer et al., 2016), although the antiviral activity, pharmacology, and toxicity of these specific molecules in humans are unknown. We therefore examined whether nucleoside analogs that show potent inhibition of hepatitis C virus (HCV), another member of the *Flaviviridae*, could inhibit ZIKV infection in NES cell cultures. An initial screen of several HCV inhibitors in Huh-7 hepatoma cells revealed that the nucleoside analog 2′-C-methyladenosine and the nucleotidyl prodrug Sofosbuvir showed antiviral activity against ZIKV, whereas Mericitabine, Balapiravir, PSI-6206, and 4′-azidocytidine analogs HY-77651 and HY-77652, lacked ZIKV antiviral activity (data not shown). Importantly, 2′-C-methyladenosine and Sofosbuvir both had potent anti-ZIKV activity in NES cells (Figures 7A and 7B). Sofosbuvir protected NES cells from ZIKV-induced cell death, whereas 2′-C-methyladenosine exhibited mild toxicity on its own (Figures 7A and 7C). Furthermore, both compounds inhibited the relocalization of pTBK1 (Figure 7D). Together, these data suggest that Sofosbuvir, a drug approved for treatment of chronic HCV, shows promise in protecting neural stem cells from ZIKV infection and pathogenesis.

DISCUSSION

The increased incidence of microcephaly linked to maternal ZIKV infection has created an international public health crisis. Understanding ZIKV cell tropism, the impact of ZIKV on cell biology, and how these effects lead to microcephaly and other neurodevelopmental phenotypes requires either direct access to developmental human brain tissue or the development of suitable model systems. In this study, we present several key advances. First, we report on the derivation and characterization of NES cells, a model system of long-term neuroepithelial stem cells derived from the NCX or SC. We also show that NES cells and RGCs are infected, mitotically impaired, and killed by ZIKV. We describe the relocation and sequestration of pTBK1 from centrosomes to mitochondria following ZIKV infection. Furthermore, we show that inhibition of TBK1 phenocopies ZIKV-infection-associated mitotic defects and supernumerary centrosomes. Finally, we found that two nucleoside analogs, one of which is an approved drug, can inhibit ZIKV replication

Figure 5. Centrosomal Depletion and Mitochondrial Sequestration of pTBK1 in ZIKV-Infected NES Cells and RGCs

(A) Violin plots of *TBK1* gene expression level in single cells from NCX-NES cells, fetal neocortical slices, and adult NCX. y axis, $\log_2$ transformed RPKM for NCX-NES cells and fetal NCX cells or $\log_2$ transformed RPM for adult NCX single cells.

(B) Digital droplet PCR (n = 3 biological replicates) shows higher *TBK1* expression in NCX-NES cells compared to organotypic slices. No differences in *TBK1* levels between ZIKV (Cambodian or Brazilian strains, $ZIKV^C$ and $ZIKV^B$, respectively) infected and Mock conditions in NCX-NES cells and fetal neocortical organotypic slices at 3.5 DPI (as well as at 1.5 DPI; data not shown). Results are presented as mean ± SD.

(C) Western blot of TBK1 and pTBK1 in VZ/SVZ and CP.

(D) Immunostaining for pTBK1 and phosphorylated VIM (pVIM) in NES cells, labeling centrosome and midbody (arrows). pTBK1 and PAX6 are expressed in fetal NCX. pTBK1 and pVIM can be detected in NES cells that are dividing. PAX6 is co-expressed with pTBK1 in VZ and SVZ of fetal NCX and labels cells that are in mitosis. Neither pTBK1 nor PAX6 are detected in CP.

(E–H) NES cells immunostaining shows that pTBK1 is colocalized with the centrosome marker TUBG (G), but not with the mitochondria marker ATP5A1 (E), in non-infected cells. Contrarily, in ZIKV-infected NES cells, pTBK1 is relocalized to mitochondria, as can be observed by co-staining of pTBK1 with ATP5A1 (F), but not with TUBG (H). Infected cells have an abnormal number of centrosomes as indicated by arrows. Arrowheads indicate mitochondrial staining, and asterisks represent multiple nuclei.

(I and J) Electron microscopy confirms the subcellular localization of pTBK1 in the centrosome (red arrows) and cytoplasm (asterisks) of non-infected cells (I). In infected cells, the signal is detected mainly in mitochondria (J), as indicated by arrowheads. ZIKV particles are also visible in the cytoplasm of infected cells (green arrows).

(K–N) Immunostaining of pTBK1 in neocortical slices shows its localization in the centrosomes and colocalization with TUBG but not with ATP5A1 in non-infected cells (K and M). In infected cells, pTBK1 is present in mitochondria (L). Infected cells in mitosis also show an abnormal number of centrosomes (N). In some infected cells with multiple centrosomes, pTBK1 and TUBG colocalize.

(O) A bar plot indicating the percentage of pTBK1 localized in centrosomes or mitochondria in mock or ZIKV conditions. pTBK1 is mainly localized in centrosomes in mock or mitochondria in ZIKV-infected cells (number of $pTBK1^+$ NES cells = 23 out of 1,364 total cells for mock and 56 out of 673 total cells for ZIKV; number of $pTBK1^+$ brain slice cells = 50 from two sections for mock and 31 from four sections for ZIKV). Data are presented as mean ± SEM. Fisher's exact test, $^{***}p < 0.001$.

(P) Jitter plot showing the number of centrosomes in $pTBK1^+$ cells in both NES cells and slice cultures. Although the number of centrosomes is predominantly 2 in non-infected mitotic cells, in infected cells, it ranges from one to five (number of $pTBK1^+$ NES cells = 40 for mock and 80 for ZIKV condition; number of $pTBK1^+$ brain slice cells = 76 from two sections for mock and 21 from four sections for ZIKV). Fisher's exact test, $^{**}p < 0.01$ and $^{***}p < 0.001$. Results are presented as mean ± SD.

(Q) Bar plot of mitochondrial area and mitochondrial density in non-infected and infected NES cells. There is a statistical significant increase in the mitochondrial area between Mock and ZIKV conditions. No difference is present between mock and ZIKV for mitochondrial density. Two-tailed t test, $^{*}p \leq 0.05$. Results are presented as mean ± SD.

(R) Representative immunofluorescence staining of vehicle-, Amlexanox-, and BX795-treated NCX-NES cells shows supernumerary centrosomes induced by TBK1 inhibition.

(S) Quantification of $pTBK1^+$ mitotic NCX-NES cells with or without TBK1 inhibition. Results are presented as mean ± SD.

Scale bars represents 20 μm (D–N) and 50 μm (R). Two-tailed t test, $^{**}p < 0.01$ and $^{***}p < 0.001$.

See also Figure S6 and S7.

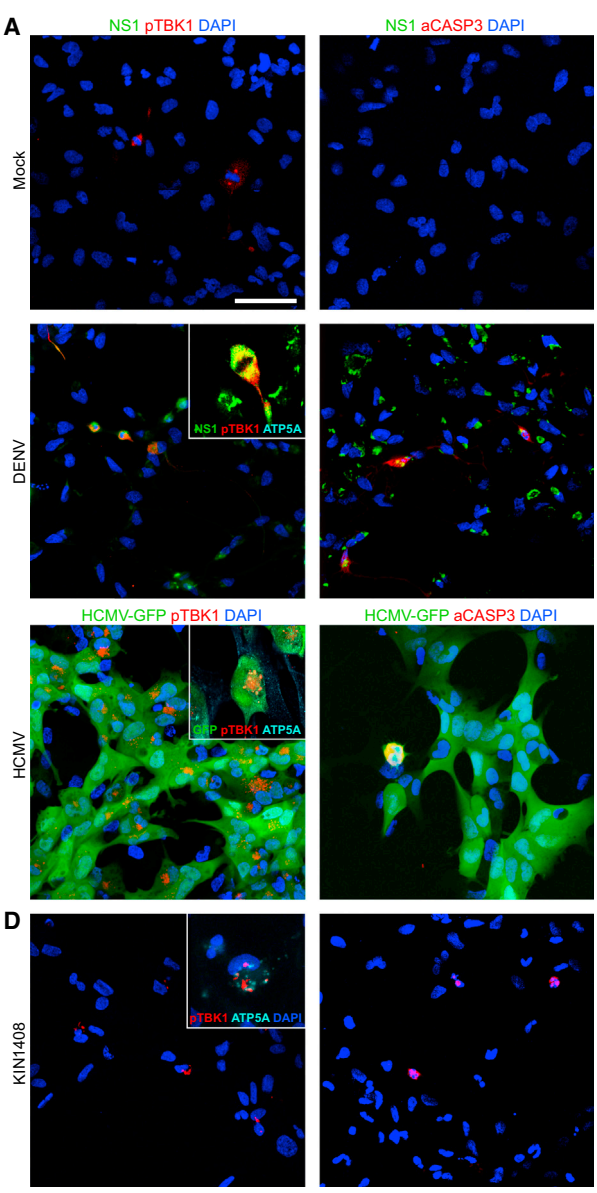

Figure 6. Relocalization of pTBK1 by Other Viruses and Innate Immune Stimulation in NES Cells

(A) Both the flavivirus dengue-2 virus (DENV) and human cytomegalovirus (HCMV) infect NCX-NES cells and induce aCASP3-mediated cell death, but only HCMV can induce relocalization of pTBK1 at 3.5 DPI.

(B) Bar plot indicating the percentage of pTBK1 that was localized in centrosomes or mitochondria in mock, DENV, or HCMV conditions (number of pTBK1$^+$ cells = 10 out of 1,074 total cells for mock, 7 out of 1,194 cells for DENV, and 392 out of 441 cells for HCMV, respectively). Fisher's exact test, ***$p < 0.001$.

(C) Bar plot of the percentage of aCASP3$^+$ cells in mock and DENV- or HCMV-infected NCX-NES cells at 3.5 DPI (number of aCASP3$^+$ cells = 1 out of 1,041 total cells for mock, 21 out of 842 cells for DENV, and 10 out of 472 cells for HCMV). Two-tailed t test, *$p < 0.05$, **$p < 0.01$.

(D) Treatment with the agonist of RIG-I-like receptors KIN1408 induces relocalization of pTBK1 from centrosomes to mitochondria and increased aCASP3-mediated cell death.

(E) Bar plot indicating the percentage of pTBK1 that was localized in centrosomes or mitochondria in vehicle- or KIN1408-treated NES cells after 2-day treatment (number of pTBK1$^+$ cells = 10 out of 1,074 total cells for vehicle and 19 out of 934 cells for KIN1408). Fisher's exact test, ***$p < 0.001$.

(F) Bar plot indicating the percentage of aCASP3$^+$ cells in vehicle- or KIN1408-treated NES cells (number of aCASP3$^+$ cells = 3 out of 1,236 total cells for vehicle and 23 out of 546 cells for KIN1408). Two-tailed t test **$p < 0.01$.

Results are presented as mean ± SD. Scale bars represent 50 μm.

and cell death in NES cells. These results are consistent with and substantially add to recent studies on ZIKV neurotropism and potential entry receptors (Miner and Diamond, 2016).

Several neurogenic populations of stem/progenitor cells have been developed from mouse or human neural tissue, but many of these culture systems have limited neurogenic and differentiation potentials (Onorati et al., 2011; Sun et al., 2008). Although recent work on hPSCs has expanded the range of neural cell types attainable (Conti and Cattaneo, 2010; Edri et al., 2015; Koch et al., 2009) and a population of NES cells has been derived from the hindbrain (Tailor et al., 2013), the NES cell system we described and characterized is, to our knowledge, the first neuropotent populations derived directly from the prospective NCX and SC, respectively. As such, NES cells represent a substantial advance facilitating the study of early development and neuropathology in the human CNS. Additionally, by conducting a comprehensive single-cell RNA-seq analysis of NES cells and human prenatal NCX specimens, including matched donor tissue, we have also generated a resource for future neuroscience and genomic studies.

By comparing our NES cells to ex vivo fetal organotypic brain slices and a ZIKV-infected fetal brain, we demonstrated definitively that RGCs are the primary cell type infected by ZIKV in the prenatal human brain, as previously suggested by using hPSC-derived neural progenitors or midfetal stem cell systems (Dang et al., 2016; Garcez et al., 2016; Qian et al., 2016; Tang et al., 2016; Lazear et al., 2016; Li et al., 2016; Cugola et al., 2016; Miner et al., 2016; Wu et al., 2016; Hanners et al., 2016; http://www.biorxiv.org/content/biorxiv/early/2016/06/15/058883.1.full.pdf). We also found that early SC stem cells can be infected by ZIKV. This is in agreement with a previous report showing SC defects in ZIKV-infected mouse models (Lazear et al., 2016) as well as a human case where descending tracts of the SC, particularly the lateral corticospinal tracts, were very affected (Mlakar et al., 2016), though this latter phenotype could be a secondary

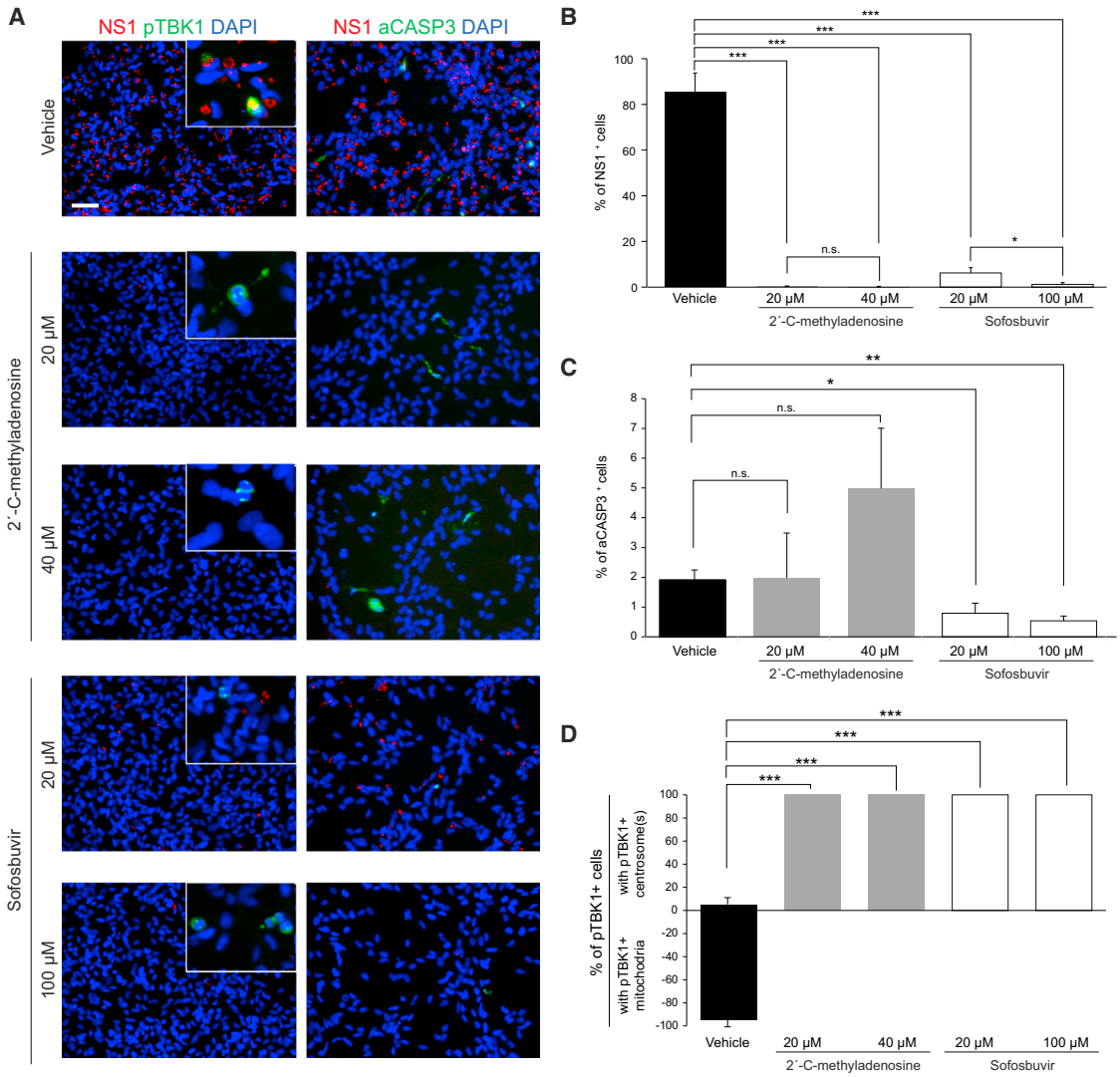

Figure 7. Nucleoside and Nucleotide Analogs Inhibit ZIKV Replication and Protect NES Cells

(A) Representative pictures showing 2′-C-methyladenosine and Sofosbuvir treatment on ZIKV-infected NES cells at 3.5 DPI. At different concentrations, both drugs show a potent anti-ZIKV activity, as demonstrated by NS1 staining. pTBK1 localization is centrosomal in infected drug-treated cells. aCASP3 staining shows apoptotic cell death rate in the different conditions.

(B) Bar plot indicating the percentage of NS1$^+$ cells in ZIKV-infected NES cells after vehicle or drug treatment at 3.5 DPI (number of NS1$^+$ cells = 2,961 out of 3,501 total cells for vehicle, 7 out of 2,118 total cells for 2′-C-methyladenosine [20μM], 2 out of 1,959 total cells for 2′-C-methyladenosine [40μM], 136 out of 2,248 total cells for Sofosbuvir [20μM], and 25 out of 2,099 total cells for Sofosbuvir [100μM]). Two-tailed t test, *$p < 0.05$ and ***$p < 0.001$. n.s., not significant.

(C) Bar plot of the percentage of aCASP3$^+$ cells in ZIKV-infected NES cells after vehicle or drug treatment at 3.5 DPI (number of aCASP3$^+$ cells = 27 out of 1,403 total cells for vehicle, 14 out of 9,55 total cells for 2′-C-methyladenosine [20 μM]); 24 out of 502 total cells for 2′-C-methyladenosine [40 μM], 5 out of 657 total cells for Sofosbuvir [20 μM], and 4 out of 727 total cells for Sofosbuvir [100 μM]).Two-tailed t test, *$p < 0.05$ and **$p < 0.01$. n.s., not significant.

(D) Bar plot indicating the percentage of pTBK1 that was localized in centrosomes or mitochondria in ZIKV-infected NES cells after vehicle or drug treatment at 3.5 DPI (number of pTBK1$^+$ cells = 32 out of 2,098 total cells for vehicle, 5 out of 1,163 total cells for 2′-C-methyladenosine [20μM], 4 out of 1,457 cells for 2′-C-methyladenosine [40μM], 13 out of 1,591 cells for Sofosbuvir [20μM], and 17 out of 1,373 total cells for Sofosbuvir [100μM]). Fisher's exact test, ***$p < 0.001$. Scale bars represent 20 μm.

Results are presented as mean ± SD.

consequence of neocortical infection. Why ZIKV infection is associated with micrencephaly rather than SC defects may in part be a result of the timing at which infection happens; human SC completes neurogenesis much earlier than the rest of the CNS (Silbereis et al., 2016), and so if infection occurs after the end of the first trimester, then SC cells may rarely be infected. However, the low percentage of neurons infected in NES cells and the fact that infected neurons in the organotypic slice cultures appeared only after the infection of VZ/SVZ RGCs suggest that some neurons may inherit the virus from infected RGCs.

We found that ZIKV infection of NES cells and RGCs caused a subcellular relocation of pTBK1 from centrosomal and cytosolic to mitochondrial locations. Consistent with its role in mitotic proliferation, pTBK1 was present in mitotic uninfected RGCs and NES cells throughout the cytoplasm and enriched at the centrosomes and midbody during cytokinesis. In contrast, we found that pTBK1 localized to mitochondria in ZIKV infected cells and was depleted in the cytoplasm and centrosomes. This is in agreement with the reported recruitment of TBK1 to the mitochondrial antiviral signaling platform in response to viral infection (Belgnaoui et al., 2011; Ning et al., 2014). Taken together, these results suggest a cell defense mechanism employed by NES cells and RGCs upon ZIKV infection that may result in abnormal mitoses. Although mitotic impairment in ZIKV infection has been described in previous reports (Garcez et al., 2016; Qian et al., 2016; Tang et al., 2016; Li et al., 2016), neither TBK1-associated centrosomal nor mitotic defects have been previously described.

Because altered cell-cycle dynamics may in some instances cause microcephaly, the removal of pTBK1 from the centrosome may explain some of the phenotypes associated with ZIKV infection. To test this hypothesis, we inhibited TBK1 by Amlexanox or BX795. Application of these inhibitors to NES cells impaired mitosis and induced supernumerary centrosomes. Multiple centrosomes and nuclei were also present in ZIKV-infected NES cells and RGCs, confirming that pTBK1 plays an important role in mitosis in these cells. Intriguingly, the majority of human microcephaly-associated genes encode centrosomal proteins (Diaz and Gleeson, 2009; Roberts et al., 2000; Woods, 2004). Moreover, studies in mutant mice and humans with mutations in centrosomal genes exhibit deficits including supernumerary centrosomes and failed cytokinesis, resulting in severely defective neurogenesis, massive apoptosis in the proliferative zones, and microcephaly (Bae et al., 2015; Diaz and Gleeson, 2009; Roberts et al., 2000; Woods, 2004).

pTBK1 is recruited to mitochondria in response to RNA virus infections, where it serves to transduce signals from MAVS protein and activate IRF-3 (Liu et al., 2015). Given that other flaviviruses induce RLR-mediated MAVS signaling (Lazear et al., 2013; Suthar et al., 2013), it is likely that mitochondrial relocalization of pTBK1 in ZIKV-infected NES cells and RGCs occurs via MAVS signaling. Supporting this possibility, treatment with KIN1408, a known RLR agonist, phenocopied both the relocalization of pTBK1 and the induction of CASP3-mediated cell death in NES cells. These data therefore support the model that ZIKV disrupts mitosis in neural stem cells by activating RLRs. Interestingly, the human TORCH pathogen, HCMV, caused a similar relocalization of pTBK1 and CASP3-mediated cell death. However, DENV, a flavivirus that inhibits RLR/MAVS/pTBK1 signaling (Dalrymple, Cimica and Mackow, 2015; He et al., 2016), did not induce pTBK1 relocalization while still resulting in apoptotic cell death. It is unlikely that the mitochondrial localization of pTBK1 alone is sufficient to explain the extensive cell death observed in more severe examples of ZIKV-infected fetal brain. The presence of uninfected RGCs exhibiting atypical cytomegalic ''balloon'' morphologies suggests that even uninfected neural cells can be non-cell-autonomously affected in response to ZIKV infection (Bell et al., 1971). Different cell types in the adult brain, including astrocytes, may be infected with ZIKV and nonetheless seem to survive for extended periods of time. In this and earlier studies in mouse models of ZIKV infection, neurons maintained normal morphology, despite being infected by ZIKV and likely survived for extended period of time. Similarly, we observed numerous RGCs and ependymal cells in ZIKV-infected postmortem human fetal NCX and SC that exhibited no obvious signs indicative of impending cell death. Crucially, these cells are either slowly dividing as neurogenesis has already ceased or are largely postmitotic, which raises the possibility that the process of mitosis, or attempting to go through mitosis in the absence of centrosomal pTBK1, may be the central mechanism underlying ZIKV-induced depletion of the neural progenitor pool and the subsequent microcephalic phenotype. Additionally, ZIKV may not affect neuronal migration even though the centrosome is critical for this process (Bae et al., 2015; Diaz and Gleeson, 2009; Woods, 2004).

We identified two nucleoside analogs, including the FDA-approved drug Sofosbuvir, that inhibit ZIKV infection and cytopathology in NES cells. Additional study is warranted to examine the efficacy of Sofosbuvir in inhibiting ZIKV in humans and test safety in pregnant women. In contrast, the TBK1 inhibitor Amlexanox, which is used clinically (Reilly et al., 2013), may exacerbate ZIKV-induced cytopathic effects.

Finally, our work may have significant implications concerning the effects of infection, the innate immune response, and the development of the CNS. The human CNS is usually considered an immunoprivileged organ and is generally protected from pathogens circulating in the rest of human body during development by the placenta (Burton and Fowden, 2015; Mor, 2016) and the forming blood-brain and blood-cerebrospinal fluid barriers (Marín-Padilla, 2012; Møllgård and Saunders, 1986). However, some pathogens, such as ZIKV, possess the ability to cross the placenta and blood-brain barriers and infect the brain. Notably, almost all congenital TORCH infections involve some aspect of neurodevelopmental defect, including retinopathy, brain calcification, and microcephaly (Fine and Arndt, 1985; Neu et al., 2015). Considering shared clinical features and the pivotal role of TBK1 in the innate immune response to viruses and in autophagic clearance of various types of pathogens (Helgason et al., 2013; Thurston et al., 2009), we found that HCMV congenital infections may disrupt the development of human CNS through overlapping mechanisms that involve altering the subcellular localization and function of pTBK1 in human neural stem cells.

Future studies are expected to dissect the role of pTBK1 in innate immune response and the exact mechanisms by which centrosomal depletion of pTBK1 is triggered in the context of RLRs/MAVS signaling. Furthermore, the functional characterization of downstream effects of pTBK1 mitochondrial activation will reveal its role in cell death and potential molecular targets in a broad scenario of viral infection.

In summary, our study shows the utility of different in vitro and ex vivo model systems of human neural stem cells for studying early neurodevelopment and ZIKV infections and reveals cellular and molecular mechanisms underlying neurodevelopmental defects associated with ZIKV infection and, potentially, other pathogens.

EXPERIMENTAL PROCEDURES

Ethics Statement

This study was conducted using de-identified postmortem human specimens from tissue collection at the Department of Neuroscience, Yale School of Medicine, and tissue specimens provided by the Human Developmental Biology Resource (www.hdbr.org) and by the Laboratory of Developmental Biology at the University of Washington. Appropriate informed consent was obtained, and all available non-identifying information was recorded for each specimen. All work was performed according to NIH guidelines for the acquisition and distribution of human tissue for bio-medical research purposes and with approval by the Human Investigation Committees and Institutional Ethics Committees of each institute from which samples were obtained. Appropriate written informed consent was obtained, and all available non-identifying information was recorded for each sample. Details of the specimens analyzed are provided in the Supplemental Information.

Human NES Cells Derivation

NES cells were derived from dorsal forebrain and SC from de-identified prenatal human specimens. In brief, tissues were dissociated until a single-cell suspension was formed. Cells were resuspended and plated into coated dishes. See the Supplemental Experimental Procedures for details.

Single-Cell RNA-Seq Analysis

Cells were captured using C1 Single-Cell Auto Prep Integrated Fluidic Circuit (Fluidigm). Single-cell sequencing libraries were generated according to manufacturer's protocol. Reads were aligned using STAR (v2.4.0). Gene expression was calculated using RSEQTools and SAMtools. See the Supplemental Experimental Procedures for details and analysis pipelines.

Ex Vivo Fetal Organotypic Slices Cultures

Neocortical walls from four fetal brains were dissected in hibernate solution. Tissue was then imbedded in agarose and sectioned. 300 μm slices were transferred to cell culture with neuronal medium. See the Supplemental Experimental Procedures for details.

Preparation of Virus Stocks

ZIKV strain FSS 13025 was obtained from the World Reference Center for Emerging Viruses and Arboviruses at University of Texas Medical Branch, Galveston. The Brazilian ZIKV strain PE243 was recovered from a 19-year-old female in Brazil in late 2015. DENV-2 strain 16681 was recovered from the cDNA clone pD2/IC-30P. See the Supplemental Experimental Procedures for details. Independent stocks of HCMV-GFP were kindly supplied by Felicia Goodrum and Scott Terhune.

ZIKV Infection of NES Cells and Fetal Organotypic Brain Slices

For NES cell infections, cells were seeded 1 day before virus addition. All viral infections were performed under the same conditions at an MOI of 0.1 for 2 hr followed by three washes and addition of fresh NES medium. For fetal organotypic brain slices, viruses were added to culture medium. See the Supplemental Experimental Procedures for details.

Application of Small-Molecule Inhibitors

Amlexanox was applied at 10 μM, BX795 at 1 μM, and KIN1408 at 10 μM (final concentration). Sofosbuvir and 2′C-methyladenosine were applied at the indicated concentrations. See the Supplemental Experimental Procedures for details.

BrdU Labeling, Immunostaining, and Electron Microscopy

10 μM BrdU was administered 30 min prior to viral infection and then continued until cell harvesting. For immunostaining, fixed samples were permeabilized and blocked at room temperature, incubated with primary antibodies overnight at 4°C, washed and incubated with secondary antibodies. All images were acquired using a fluorescent microscopy or a laser scanning confocal microscope. For detailed methods and electron microscopy. see the Supplemental Experimental Procedures.

RNA Isolation, Droplet Digital PCR, and Immunoblotting

Total RNA or proteins were extracted from mock and infected samples as described in Supplemental Experimental Procedures.

Statistical Analysis

The presented data are mean ± SD or SEM from three separate experiments. Differences between the groups were analyzed using a Student's t test. Values of all significant correlations are given with degree of significance indicated (* $p \leq 0.05$, ** $p < 0.01$, and *** $p < 0.001$). For organotypic slice culture, quantification was performed in up to four sections that were representative of at least three slices. Cells were counted as described in the respective figure legend. The number of cells with pTBK1 located in centrosomes or mitochondria follows a binomial distribution. A Fisher's exact test was performed in order to compare the control and the infected and treated group. Similarly, to test whether infection changed the number of centrosomes, the cells were binned by the number of centrosomes (1–5), and a Fisher's exact test was performed in order to compare control with infected and treated cells.

ACCESSION NUMBERS

The accession number for single-cell RNA-seq data reported in this paper is NCBI GEO: GSE81475. The accession number for the Brazilian ZIKV strain PE243 is GenBank: KX197192.

SUPPLEMENTAL INFORMATION

Supplemental Information contains Supplemental Experimental Procedures, seven figures, and four tables and can be found with this article online at http://dx.doi.org/10.1016/j.celrep.2016.08.038.

AUTHOR CONTRIBUTIONS

T.L.H., B.D.L., and N.S. conceived the research and contributed to the design of the study and analysis of the data. M.O., Z.L., F.L., A.M.M.S., B.D.L., and N.S. designed and performed most of the ZIKV infection experiments. M.O., F.L., and M.T.D.A. derived and characterized NES cells. S.L. collected human brain specimens for NES derivation. Z.L. and T.G. generated single-cell RNA-seq data. Z.L. and M.L. performed RNA-seq analyses. M.P., J.M, A.M.M.S., M.P., N.N., A.T., and E.S.A. analyzed the ZIKV-infected human brain. S.P., A.T.N.T., T.D., W.H., F.G., Y.Z., C.B., T.G., K.S.-B., L.V., Y.Z., X.-B. G., S.M.S., and L.K.K. contributed to additional data collection and analyses. M.F. provided NS1 monoclonal antibody and technical inputs. M.O., Z.L., F.L., A.M.M.S., F.G., C.B., B.D.L., and N.S. wrote the first draft of the manuscript and prepared figures. All authors edited the manuscript.

ACKNOWLEDGMENTS

We thank Carolyn Hain for assistance with tissue acquisition and processing and Brian G. Rash for technical advice. We also thank Angeliki Louvi and Flora Vaccarino for sharing equipment and providing reagents and tissue samples. We thank Alain Kohl (MRC Glasgow) for providing us with the Brazilian ZIKV strain PE243, Scott Terhune (Medical College of Wisconsin) and Felicia Goodrum (University of Arizona) for supplying HCMV-GFP, and Avinash Phadke (Achillion Pharmaceuticals) for supplying samples of Sofosbuvir and 2′-C-methyladenosine. We also thank the other members of our laboratories for their comments. This work was supported by grants NS076503, MH103339, MH105972, MH106934, MH060929, NS080388, AG034924, AG047270, DC01919, AI120113, and AI089826 from the NIH, SFARI 307705 from the Simons Foundation, and 15-RMA-YALE-31 from Connecticut Innovations' Regenerative Medicine Research Fund. The Laboratory of Developmental Biology at the University of Washington, Seattle, and Human Developmental Biology Resource were supported by NIH award number HD0008836 and the Joint MRC/Wellcome Trust grant 099175/Z/12/Z, respectively. Additional support was provided by the Kavli Foundation and the Falk Medical Research Trust.

Received: May 16, 2016
Revised: July 27, 2016
Accepted: August 12, 2016
Published: August 24, 2016

REFERENCES

Adams Waldorf, K.M., and McAdams, R.M. (2013). Influence of infection during pregnancy on fetal development. Reproduction *146*, R151–R162.

Araujo, A.Q., Silva, M.T., and Araujo, A.P. (2016). Zika virus-associated neurological disorders: a review. Brain *139*, 2122–2130.

Bae, B.I., Jayaraman, D., and Walsh, C.A. (2015). Genetic changes shaping the human brain. Dev. Cell *32*, 423–434.

Barrows, N.J., Campos, R.K., Powell, S.T., Prasanth, K.R., Schott-Lerner, G., Soto-Acosta, R., Galarza-Muñoz, G., McGrath, E.L., Urrabaz-Garza, R., Gao, J., et al. (2016). A screen of fda-approved drugs for inhibitors of zika virus infection. Cell Host Microbe *20*, 259–270.

Belgnaoui, S.M., Paz, S., and Hiscott, J. (2011). Orchestrating the interferon antiviral response through the mitochondrial antiviral signaling (MAVS) adapter. Curr. Opin. Immunol. *23*, 564–572.

Bell, T.M., Field, E.J., and Narang, H.K. (1971). Zika virus infection of the central nervous system of mice. Arch. Gesamte Virusforsch. *35*, 183–193.

Brasil, P., Sequeira, P.C., Freitas, A.D., Zogbi, H.E., Calvet, G.A., de Souza, R.V., Siqueira, A.M., de Mendonca, M.C.L., Nogueira, R.M.R., de Filippis, A.M.B., and Solomon, T. (2016). Guillain-Barré syndrome associated with Zika virus infection. Lancet *387*, 1482.

Broutet, N., Krauer, F., Riesen, M., Khalakdina, A., Almiron, M., Aldighieri, S., Espinal, M., Low, N., and Dye, C. (2016). Zika Virus as a cause of neurologic disorders. N. Engl. J. Med. *374*, 1506–1509.

Burton, G.J., and Fowden, A.L. (2015). The placenta: a multifaceted, transient organ. Philos. Trans. R. Soc. Lond. B Biol. Sci. *370*, 20140066.

Conti, L., and Cattaneo, E. (2010). Neural stem cell systems: physiological players or in vitro entities? Nat. Rev. Neurosci. *11*, 176–187.

Cugola, F.R., Fernandes, I.R., Russo, F.B., Freitas, B.C., Dias, J.L.M., Guimarães, K.P., Benazzato, C., Almeida, N., Pignatari, G.C., Romero, S., et al. (2016). The Brazilian Zika virus strain causes birth defects in experimental models. Nature *534*, 267–271.

Dalrymple, N.A., Cimica, V., and Mackow, E.R. (2015). Dengue virus ns proteins inhibit rig-i/mavs signaling by blocking tbk1/irf3 phosphorylation: dengue virus serotype 1 ns4a is a unique interferon-regulating virulence determinant. MBio *6*, e00553–e15.

Dang, J., Tiwari, S.K., Lichinchi, G., Qin, Y., Patil, V.S., Eroshkin, A.M., and Rana, T.M. (2016). Zika virus depletes neural progenitors in human cerebral organoids through activation of the innate immune receptor TLR3. Cell Stem Cell *19*, 258–265.

Darmanis, S., Sloan, S.A., Zhang, Y., Enge, M., Caneda, C., Shuer, L.M., Hayden Gephart, M.G., Barres, B.A., and Quake, S.R. (2015). A survey of human brain transcriptome diversity at the single cell level. Proc. Natl. Acad. Sci. USA *112*, 7285–7290.

de Paula Freitas, B., de Oliveira Dias, J.R., Prazeres, J., Sacramento, G.A., Ko, A.I., Maia, M., and Belfort, R., Jr. (2016). Ocular findings in infants with microcephaly associated with presumed Zika virus congenital infection in salvador, Brazil. JAMA Ophthalmol. *134*, 529–535.

Diaz, A.L., and Gleeson, J.G. (2009). The molecular and genetic mechanisms of neocortex development. Clin. Perinatol. *36*, 503–512.

Edri, R., Yaffe, Y., Ziller, M.J., Mutukula, N., Volkman, R., David, E., Jacob-Hirsch, J., Malcov, H., Levy, C., Rechavi, G., et al. (2015). Analysing human neural stem cell ontogeny by consecutive isolation of Notch active neural progenitors. Nat. Commun. *6*, 6500.

Elkabetz, Y., Panagiotakos, G., Al Shamy, G., Socci, N.D., Tabar, V., and Studer, L. (2008). Human ES cell-derived neural rosettes reveal a functionally distinct early neural stem cell stage. Genes Dev. *22*, 152–165.

Eyer, L., Nencka, R., Huvarová, I., Palus, M., Joao Alves, M., Gould, E.A., De Clercq, E., and Růžek, D. (2016). Nucleoside inhibitors of zika virus. J. Infect. Dis. *214*, 707–711.

Farlik, M., Rapp, B., Marie, I., Levy, D.E., Jamieson, A.M., and Decker, T. (2012). Contribution of a TANK-binding kinase 1-interferon (IFN) regulatory factor 7 pathway to IFN-γ-induced gene expression. Mol. Cell. Biol. *32*, 1032–1043.

Fine, J.D., and Arndt, K.A. (1985). The TORCH syndrome: a clinical review. J. Am. Acad. Dermatol. *12*, 697–706.

Gage, F.H., and Temple, S. (2013). Neural stem cells: generating and regenerating the brain. Neuron *80*, 588–601.

Garcez, P.P., Loiola, E.C., Madeiro da Costa, R., Higa, L.M., Trindade, P., Delvecchio, R., Nascimento, J.M., Brindeiro, R., Tanuri, A., and Rehen, S.K. (2016). Zika virus impairs growth in human neurospheres and brain organoids. Science *352*, 816–818.

Hamel, R., Dejarnac, O., Wichit, S., Ekchariyawat, P., Neyret, A., Luplertlop, N., Perera-Lecoin, M., Surasombatpattana, P., Talignani, L., Thomas, F., et al. (2015). Biology of Zika Virus Infection in Human Skin Cells. J. Virol. *89*, 8880–8896.

Hanners, N.W., Eitson, J.L., Usui, N., Richardson, R.B., Wexler, E.M., Konopka, G., and Schoggins, J.W. (2016). Western zika virus in human fetal neural progenitors persists long term with partial cytopathic and limited immunogenic effects. Cell Rep. *15*, 2315–2322.

He, Z., Zhu, X., Wen, W., Yuan, J., Hu, Y., Chen, J., An, S., Dong, X., Lin, C., Yu, J., et al. (2016). Dengue virus subverts host innate immunity by targeting adaptor protein MAVS. J. Virol. *90*, 7219–7230.

Helgason, E., Phung, Q.T., and Dueber, E.C. (2013). Recent insights into the complexity of Tank-binding kinase 1 signaling networks: the emerging role of cellular localization in the activation and substrate specificity of TBK1. FEBS Lett. *587*, 1230–1237.

Kang, H.J., Kawasawa, Y.I., Cheng, F., Zhu, Y., Xu, X., Li, M., Sousa, A.M.M., Pletikos, M., Meyer, K.A., Sedmak, G., et al. (2011). Spatio-temporal transcriptome of the human brain. Nature *478*, 483–489.

Koch, P., Opitz, T., Steinbeck, J.A., Ladewig, J., and Brüstle, O. (2009). A rosette-type, self-renewing human ES cell-derived neural stem cell with potential for in vitro instruction and synaptic integration. Proc. Natl. Acad. Sci. USA *106*, 3225–3230.

Krumlauf, R., Marshall, H., Studer, M., Nonchev, S., Sham, M.H., and Lumsden, A. (1993). Hox homeobox genes and regionalisation of the nervous system. J. Neurobiol. *24*, 1328–1340.

Lazear, H.M., Lancaster, A., Wilkins, C., Suthar, M.S., Huang, A., Vick, S.C., Clepper, L., Thackray, L., Brassil, M.M., Virgin, H.W., et al. (2013). IRF-3, IRF-5, and IRF-7 coordinately regulate the type I IFN response in myeloid dendritic cells downstream of MAVS signaling. PLoS Pathog. *9*, e1003118.

Lazear, H.M., Govero, J., Smith, A.M., Platt, D.J., Fernandez, E., Miner, J.J., and Diamond, M.S. (2016). A Mouse Model of Zika Virus Pathogenesis. Cell Host Microbe *19*, 720–730.

Li, C., Xu, D., Ye, Q., Hong, S., Jiang, Y., Liu, X., Zhang, N., Shi, L., Qin, C.-F., and Xu, Z. (2016). Zika virus disrupts neural progenitor development and leads to microcephaly in mice. Cell Stem Cell *19*, 120–126.

Liu, S., Cai, X., Wu, J., Cong, Q., Chen, X., Li, T., Du, F., Ren, J., Wu, Y.-T., Grishin, N.V., and Chen, Z.J. (2015). Phosphorylation of innate immune adaptor proteins MAVS, STING, and TRIF induces IRF3 activation. Science *347*, aaa2630.

Lui, J.H., Hansen, D.V., and Kriegstein, A.R. (2011). Development and evolution of the human neocortex. Cell *146*, 18–36.

Marín-Padilla, M. (2012). The human brain intracerebral microvascular system: development and structure. Front. Neuroanat. *6*, 38.

Miner, J.J., and Diamond, M.S. (2016). Understanding how Zika virus enters and infects neural target cells. Cell Stem Cell *18*, 559–560.

Miner, J.J., Cao, B., Govero, J., Smith, A.M., Fernandez, E., Cabrera, O.H., Garber, C., Noll, M., Klein, R.S., Noguchi, K.K., et al. (2016). Zika virus infection

during pregnancy in mice causes placental damage and fetal demise. Cell *165*, 1081–1091.

Mlakar, J., Korva, M., Tul, N., Popović, M., Poljšak-Prijatelj, M., Mraz, J., Kolenc, M., Resman Rus, K., Vesnaver Vipotnik, T., Fabjan Vodušek, V., et al. (2016). Zika virus associated with microcephaly. N. Engl. J. Med. *374*, 951–958.

Møllgård, K., and Saunders, N.R. (1986). The development of the human blood-brain and blood-CSF barriers. Neuropathol. Appl. Neurobiol. *12*, 337–358.

Mor, G. (2016). Placental inflammatory response to Zika virus may affect fetal brain development. Am. J. Reprod. Immunol. *75*, 421–422.

Neu, N., Duchon, J., and Zachariah, P. (2015). TORCH infections. Clin. Perinatol. *42*, 77–103, viii.

Ning, Y.-J., Wang, M., Deng, M., Shen, S., Liu, W., Cao, W.-C., Deng, F., Wang, Y.-Y., Hu, Z., and Wang, H. (2014). Viral suppression of innate immunity via spatial isolation of TBK1/IKKε from mitochondrial antiviral platform. J. Mol. Cell Biol. *6*, 324–337.

Nowakowski, T.J., Pollen, A.A., Di Lullo, E., Sandoval-Espinosa, C., Bershteyn, M., and Kriegstein, A.R. (2016). Expression analysis highlights AXL as a candidate Zika virus entry receptor in neural stem cells. Cell Stem Cell *18*, 591–596.

Oehler, E., Watrin, L., Larre, P., Leparc-Goffart, I., Lastere, S., Valour, F., Baudouin, L., Mallet, H., Musso, D., and Ghawche, F. (2014). Zika virus infection complicated by Guillain-Barre syndrome–case report, French Polynesia, December 2013. Euro Surveill. *19*, 19.

Onorati, M., Binetti, M., Conti, L., Camnasio, S., Calabrese, G., Albieri, I., Di Febo, F., Toselli, M., Biella, G., Martynoga, B., et al. (2011). Preservation of positional identity in fetus-derived neural stem (NS) cells from different mouse central nervous system compartments. Cell. Mol. Life Sci. *68*, 1769–1783.

Onorati, M., Castiglioni, V., Biasci, D., Cesana, E., Menon, R., Vuono, R., Talpo, F., Laguna Goya, R., Lyons, P.A., Bulfamante, G.P., et al. (2014). Molecular and functional definition of the developing human striatum. Nat. Neurosci. *17*, 1804–1815.

Pattabhi, S., Wilkins, C.R., Dong, R., Knoll, M.L., Posakony, J., Kaiser, S., Mire, C.E., Wang, M.L., Ireton, R.C., Geisbert, T.W., et al. (2016). Targeting innate immunity for antiviral therapy through small molecule agonists of the rlr pathway. J. Virol. *90*, 2372–2387.

Pillai, S., Nguyen, J., Johnson, J., Haura, E., Coppola, D., and Chellappan, S. (2015). Tank binding kinase 1 is a centrosome-associated kinase necessary for microtubule dynamics and mitosis. Nat. Commun. *6*, 10072.

Qian, X., Nguyen, H.N., Song, M.M., Hadiono, C., Ogden, S.C., Hammack, C., Yao, B., Hamersky, G.R., Jacob, F., Zhong, C., et al. (2016). Brain-region-specific organoids using mini-bioreactors for modeling ZIKV exposure. Cell *165*, 1238–1254.

Reilly, S.M., Chiang, S.-H., Decker, S.J., Chang, L., Uhm, M., Larsen, M.J., Rubin, J.R., Mowers, J., White, N.M., Hochberg, I., et al. (2013). An inhibitor of the protein kinases TBK1 and IKK-ε improves obesity-related metabolic dysfunctions in mice. Nat. Med. *19*, 313–321.

Roberts, M.R., Bittman, K., Li, W.W., French, R., Mitchell, B., LoTurco, J.J., and D'Mello, S.R. (2000). The flathead mutation causes CNS-specific developmental abnormalities and apoptosis. J. Neurosci. *20*, 2295–2306.

Rubin, E.J., Greene, M.F., and Baden, L.R. (2016). Zika virus and microcephaly. N. Engl. J. Med. *374*, 984–985.

Schuler-Faccini, L., Ribeiro, E.M., Feitosa, I.M.L., Horovitz, D.D.G., Cavalcanti, D.P., Pessoa, A., Doriqui, M.J.R., Neri, J.I., Neto, J.M. de P., Wanderley, H.Y.C., et al.; Brazilian Medical Genetics Society–Zika Embryopathy Task Force (2016). Possible association between Zika virus infection and microcephaly - Brazil, 2015. MMWR Morb. Mortal. Wkly. Rep. *65*, 59–62.

Silbereis, J.C., Pochareddy, S., Zhu, Y., Li, M., and Sestan, N. (2016). The cellular and molecular landscapes of the developing human central nervous system. Neuron *89*, 248–268.

Sun, Y., Pollard, S., Conti, L., Toselli, M., Biella, G., Parkin, G., Willatt, L., Falk, A., Cattaneo, E., and Smith, A. (2008). Long-term tripotent differentiation capacity of human neural stem (NS) cells in adherent culture. Mol. Cell. Neurosci. *38*, 245–258.

Suthar, M.S., Brassil, M.M., Blahnik, G., McMillan, A., Ramos, H.J., Proll, S.C., Belisle, S.E., Katze, M.G., and Gale, M., Jr. (2013). A systems biology approach reveals that tissue tropism to West Nile virus is regulated by antiviral genes and innate immune cellular processes. PLoS Pathog. *9*, e1003168.

Tailor, J., Kittappa, R., Leto, K., Gates, M., Borel, M., Paulsen, O., Spitzer, S., Karadottir, R.T., Rossi, F., Falk, A., and Smith, A. (2013). Stem cells expanded from the human embryonic hindbrain stably retain regional specification and high neurogenic potency. J. Neurosci. *33*, 12407–12422.

Tang, H., Hammack, C., Ogden, S.C., Wen, Z., Qian, X., Li, Y., Yao, B., Shin, J., Zhang, F., Lee, E.M., et al. (2016). Zika virus infects human cortical neural progenitors and attenuates their growth. Cell Stem Cell *18*, 587–590.

Thurston, T.L.M., Ryzhakov, G., Bloor, S., von Muhlinen, N., and Randow, F. (2009). The TBK1 adaptor and autophagy receptor NDP52 restricts the proliferation of ubiquitin-coated bacteria. Nat. Immunol. *10*, 1215–1221.

Woods, C.G. (2004). Human microcephaly. Curr. Opin. Neurobiol. *14*, 112–117.

Wu, K.-Y., Zuo, G.-L., Li, X.-F., Ye, Q., Deng, Y.-Q., Huang, X.-Y., Cao, W.-C., Qin, C.-F., and Luo, Z.-G. (2016). Vertical transmission of Zika virus targeting the radial glial cells affects cortex development of offspring mice. Cell Res. *26*, 645–654.

Zhang, Y., Sloan, S.A., Clarke, L.E., Caneda, C., Plaza, C.A., Blumenthal, P.D., Vogel, H., Steinberg, G.K., Edwards, M.S.B., Li, G., et al. (2016). Purification and characterization of progenitor and mature human astrocytes reveals transcriptional and functional differences with mouse. Neuron *89*, 37–53.

Zmurko, J., Marques, R.E., Schols, D., Verbeken, E., Kaptein, S.J.F., and Neyts, J. (2016). The viral polymerase inhibitor 7-deaza-2′-c-methyladenosine is a potent inhibitor of in vitro zika virus replication and delays disease progression in a robust mouse infection model. PLoS Negl. Trop. Dis. *10*, e0004695.